Sustainable Cities and Society 131 (2025) 106629

Contents lists available at ScienceDirect

Sustainable Cities and Society

journal homepage: www.elsevier.com/locate/scs

Reanalysis-data-based approach to generate urban local weather data to support building energy design in a tropical climate

Xing Zheng [a,b], Naika Meili [b], Shuyang Li [b,c], Huanhuan Wang [d], Lei Xu [b,e], Zhen Han [f], Martín Mosteiro-Romero [g], Yi Wu [h], Da Yan [h], Dengkai Chi [b], Guanli Feng [a,c,*], Rudi Stouffs [c]

[a] Department of Architecture and Civil Engineering, City University of Hong Kong, Hong Kong SAR, China
[b] Future Cities Laboratory Global, Singapore-ETH Centre, Singapore
[c] Department of Architecture, National University of Singapore, Singapore
[d] School of Civil and Environmental Engineering, Cornell University, Ithaca, NY, USA
[e] Department of Architecture, University of Cambridge, UK
[f] Department of Architecture, Tianjin University, China
[g] Department of Architectural Engineering and Technology, TU Delft, Netherlands
[h] Department of Architecture, Tsinghua University, China

ARTICLE INFO

Keywords:
Urban microclimate
Weather data
Urban canopy model
Building energy simulation
Atmospheric reanalysis data

ABSTRACT

Accurate weather data is essential for building energy modeling (BEM), yet the actual urban local weather condition is often overlooked. This study developed an approach to generate local weather data using ERA5, a global atmospheric reanalysis dataset as input for two urban land surface models, Urban Tethys-Chloris (UT&C) and Urban Weather Generator (UWG). The generated datasets (UT&C-ERA5 and UWG-ERA5) are compared to locally measured weather data for a university campus in Singapore. Results show that the original ERA5 underestimates the diurnal temperature range. UT&C-ERA5 significantly improves hourly dry bulb temperature, reducing Mean Absolute Error (MAE) from 1.73 to 1.32 and Root Mean Square Error (RMSE) from 2.31 to 1.67, while UWG-ERA5 shows modest improvements (MAE from 1.73 to 1.70, RMSE from 2.31 to 2.22). UT&C-ERA5 also improves wind speed, lowering MAE from 2.85 to 1.54 and RMSE from 3.23 to 1.79. Subsequently, these weather datasets are employed as inputs for a calibrated BEM. Compared to the original ERA5, UT&C-ERA5 reduces CV (RMSE) of building cooling load from 17.13 % to 15.45 %. By leveraging the global availability of atmospheric reanalysis datasets, this approach can support building energy design and improve energy efficiency in tropical cities.

1. Introduction

The building sector accounts for a significant portion of global energy consumption, contributing approximately one-third of the total energy consumed by end-users (International Renewable Energy Agency, 2023). Meanwhile, CO_2 emissions from the building sector account for about one-third of the overall energy system emissions, encompassing both building operations (26 %) and embodied emissions (7 %) (International Renewable Energy Agency, 2023). These impacts are more evident in tropical countries. For example, in Singapore, buildings were responsible for consuming more than half of the total electricity supply (Energy Market Authority, 2024). The combined effects of urbanization and climate change are also expected to further magnify energy demands (Ibrahim et al., 2025; Liu et al., 2023; Shen & Yang, 2020; Shen et al., 2025; Shen, 2025; Shen et al., 2025). The Singapore government has set an ambitious target to reduce energy use intensities by 35 % by 2030 compared to the 2005 level (Duarte et al., 2017).

Building energy modeling (BEM) tools have been developed to predict building energy use and improve thermal performance. These tools rely on accurate weather data as an essential input, including temperature, humidity, solar radiation, and wind speed. The importance of weather data has been shown in BEM simulations in different climate regions (Allegrini et al., 2012; Bre et al., 2021; Chang et al., 2024; De

* Corresponding author at: City University of Hong Kong, Tat Chee Avenue, Kowloon, Hong Kong Special Administrative Region of China.
E-mail address: e0954452@u.nus.edu (G. Feng).

https://doi.org/10.1016/j.scs.2025.106629
Received 9 January 2025; Received in revised form 26 June 2025; Accepted 9 July 2025
Available online 10 July 2025

Masi et al., 2021; M'Saouri El Bat et al., 2021; Silvero et al., 2019). Typically, users source weather data from the software's built-in datasets from meteorological stations. For example, a common practice in BEM is to employ Typical Meteorological Year (TMY) data, a dataset derived from extensive historical weather observations, as the standard approach. Recently, researchers have explored alternative sources, such as global atmospheric reanalysis datasets (Liu et al., 2024; Wu et al., 2023). The global atmospheric reanalysis datasets combine past short-range weather forecasts with observations through data assimilation, which provides the most complete picture currently possible of past weather and climate. Two prominent atmospheric reanalysis datasets widely used by the scientific community are fifth-generation reanalysis data from the European Centre for Medium-Range Weather Forecasts (ERA5) (Energy Market Authority, 2025) and Modern-Era Retrospective Analysis for Research and Applications, Version 2 (MERRA-2) (Erdman, 2025). In recent years, scholars have undertaken studies across diverse fields utilizing atmospheric reanalysis datasets. For example, the ERA5 dataset has been used for the estimation of precipitation (Jiang et al., 2021; Jiao et al., 2021; Miniandi et al., 2024) and the assessment of wind resources (Gualtieri, 2021).

However, directly using TMY data, weather data from meteorological stations, or atmospheric reanalysis data for BEM presents several challenges. Firstly, TMY derived from historical data can become outdated over time, making it inadequate for representing recent weather conditions (Bourikas et al., 2016; Cui et al., 2017; Qian et al., 2023). Secondly, meteorological stations are often located in airports or rural areas, which may differ significantly from the urban environments under investigation (Hu et al., 2024; Liu et al., 2023). Thirdly, the spatial resolution of global atmospheric reanalysis datasets is generally coarse relative to cities, limiting their accuracy in capturing local climate effects (Hersbach, 2024). The use of the atmospheric reanalysis datasets has shown discrepancies with observed weather data. For example, the atmospheric reanalysis dataset systematically produced lower wind speeds than those observed across countries (Cannon et al., 2015).

Meanwhile, the influence of urban local climates on building energy demand has been widely recognized (Ignatius et al., 2016; Tian et al., 2024; Zhang et al., 2024). For instance, neglecting the Urban Heat Island (UHI) effect, which causes higher temperatures in urban areas, can significantly underestimate cooling energy usage in hot climate zones (Palme et al., 2017; Sun & Augenbroe, 2014). A study showed that considering the effect of UHI results in the prediction of energy consumption in Singapore increasing from 3.25 % to 11 % (Liu et al., 2017). By integrating the influence of local anthropogenic heat emission (Mei & Yuan, 2021; Yuan et al., 2020), a recent study has developed microclimate data for BEM (Xu et al., 2022). In this study, BEM predictions utilizing this data exhibit a mean bias error of 6 %, in contrast to 12 % when TMY data are utilized, compared to actual energy usage.

To address the limitation of directly using data from meteorological stations or atmospheric reanalysis datasets, researchers have developed methodologies to generate urban local climate datasets for BEM (Allegrini et al., 2012; Dougherty & Jain, 2023; Hashemi et al., 2024; Li et al., 2023; Li et al., 2024; Wong et al., 2021). Computational fluid dynamics (CFD) simulations and urban land surface models have been utilized to capture local weather and improve the accuracy of building energy simulations. The high-resolution local weather data from CFD has been employed as boundary conditions in BEM (Brozovsky et al., 2022; Gobakis & Kolokotsa, 2017; Hadavi & Pasdarshahri, 2021; Hadavi & Pasdarshahri, 2021; Kamal et al., 2021; Miguel et al., 2021; Miller et al., 2017; Shan et al., 2020; Toparlar et al., 2018; Yang et al., 2012; Zhang & Gao, 2021; Zhang & Mirzaei, 2020). Nonetheless, it's worth noting that CFD simulations are temporally and computationally intensive, and often focus on a few typical days, while BEM requires long-term weather data for comprehensive performance analysis. Non-CFD approaches have been suggested as alternative methods to generate localized weather data for BEM by employing parametric interpretations of urban areas (Barlow et al., 2017; Grimmond et al., 2009). Urban land surface models, which adhere to the energy conservation law and consider energy exchanges between urban surfaces and the surrounding air in street canyons, are available for parameterizing urban surface-atmosphere interactions (Lipson et al., 2023; Paolini & Santamouris, 2023). It has the advantage of rapidly generating local weather data (Detommaso et al., 2021; Jin et al., 2020). For example, Urban Weather Generator (UWG) (Bueno et al., 2012), a widely used urban land surface model, has been employed to transfer weather data for the urban context based on measured data from suburban meteorological stations, resulting in a better-predicted cooling-energy use intensity in Nanjing, China (Yang et al., 2023). UWG has also served as an input for urban scale energy modeling in Qatar, resulting in better accuracy of energy prediction compared with rural weather input (Kamal et al., 2021). In addition, fast generation of microclimate weather data for building simulation under heat islands has been developed based on UWG (Shen et al., 2021). Efforts have also been made to develop weather data for future scenarios in Shenzhen, China (Shen et al., 2023). ERA5 data was used with Surface Urban Energy and Water Balance Scheme, an urban land surface model for simulating the surface energy and hydrological fluxes (Järvi et al., 2011), to obtain an urban typical meteorological year in London for BEM . Another recent study utilized ERA5 to force a Standalone Urban Energy/Climate Model in Abu Dhabi (Afshari, 2023).

The influence of the urban elements on the local weather conditions strongly depends on the climate zones (Aliabadi et al., 2023; Hashemi et al., 2024; Wang et al., 2022; Yuan et al., 2022). Local weather data generated by urban land surface models have been employed in various cities; however, there is still limited attention devoted to cities in tropical climates. Moreover, a comparative analysis of the performance of different urban land surface models for generating local weather data tailored for building energy simulations remains unexplored. An evaluation of their performance in tropical cities has not yet been conducted. Therefore, this study focuses on generating local weather data in tropical urban climates using urban land surface models, and evaluating their performance for building energy modeling.

The remaining article is organized as follows: The methodology is illustrated in Section 2, including site information, weather data sources, and urban land surface models. The BEM and its calibration are presented in Section 3. Section 4 provides the results of performance by all the datasets, including meteorological parameters and building cooling load simulation. Several discussions from the key findings and conclusions are presented in the last two sections.

2. Methodology

We established a workflow that consists of three major steps (Fig. 1). In Step 1, we collected weather datasets. For further comparison among these datasets, we unify the meteorological parameters and determine the locally measured benchmark herein. In Step 2, a local educational building model is calibrated using EnergyPlus and adopted as BEM for the evaluation of multiple weather datasets. In Step 3, comparisons and evaluations are conducted among the weather datasets themselves and simulation results using different weather inputs in order to clarify the appropriate weather generation for building energy simulation in urban areas.

2.1. Site and local weather data

Singapore is an island state located near the equator with a typical hot and humid equatorial climate with uniformly high monthly mean air temperature and high annual precipitation of 2300 mm (Aydin et al., 2024; Jiang et al., 2021). This study selected the SDE2 building, a typical educational building located on the campus of the National University of Singapore. This building is equipped with a cooling system that uses a centralized chilled water system with water-cooled chillers. The system has a water loop that connects to cooling towers on the building's roof to

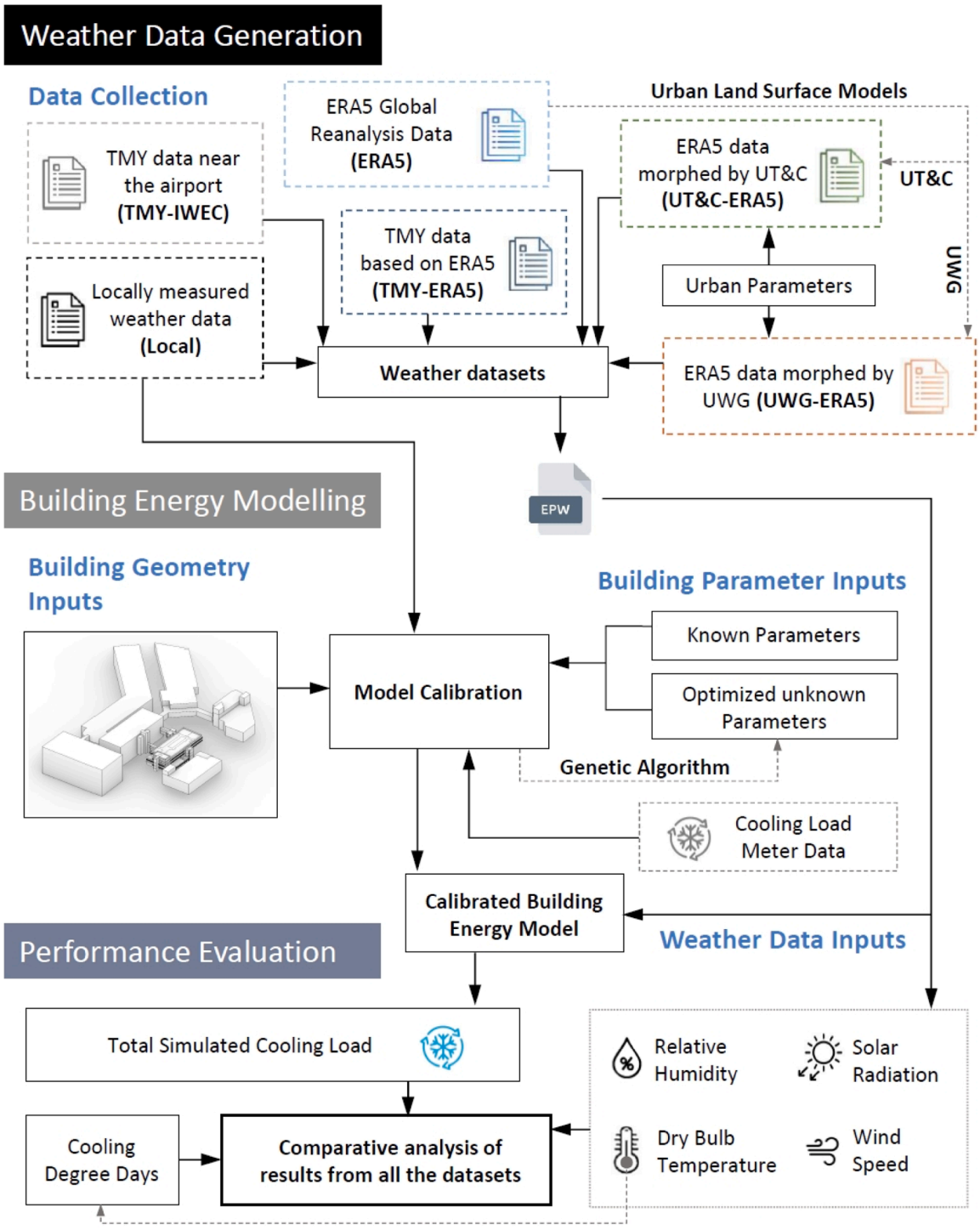

Fig. 1. Overall research workflow.

release heat. The local weather data was measured in 2019 from Feb 1st to Dec 31st, at the bus stop near the Information Technology building, which is approximately 180 m away from SDE2 building (Fig. 2(b)). The devices and their ranges used in the measurements of meteorological parameters are listed in Table 1. Temperature and humidity data are measured at about 2 m above ground level. Wind speed, wind direction, and global solar radiation data are measured at about 4 m above ground level on the roof of a bus stop without obstructions from above. Direct normal radiation and diffuse solar radiation are necessary for BEM. Therefore, the global solar radiation is partitioned using a weather generator to obtain direct and diffuse solar radiation (Fatichi et al., 2011; Meili et al., 2020).

TMY data collected from International Weather for Energy Calculations (IWEC), v2.0, is used for comparison. This data was obtained from data over 644 months at a meteorological station near Changi Airport (Huang et al., 2014), which is about 24.31 km away from SDE2 building. The location is shown in Fig. 2(a).

2.2. Reanalysis datasets

In this study, we use the European Centre Reanalysis version 5 (ERA5) data as our source of meteorological parameters (Hersbach et al.,

Fig. 2. Location of data collection (a) Satellite map of Singapore highlighting the location of the study area and the meteorological station for TMY-IWEC, (b) 3D view of SDE2 building and the bus stop at the building of Information Technology where the local weather data was measured.

Table 1
Information on the measurement of the local weather data.

Meteorological parameter	Measurement device	Measurement range
Dry bulb temperature	ONSET S-THB-M00x temperature smart sensor	−40 °C to 75 °C
Relative humidity	ONSET S-THB-M00x RH smart sensor	0–100 %
Global horizontal solar irradiance	ONSET S-LIB-M003 silicon pyranometer smart sensor	0 to 1280 W/m^2
Horizontal wind speed	YOUNG Wind Monitor-AQ Model 05,305	0–50 m/s
Precipitation	ONSET S-RGB-M002 rainfall smart sensor	0–127 mm per hour

2020). The ERA5 dataset integrates actual observations with the European Centre for Medium-Range Weather Forecasts (ECMWF) Integrated Forecasting System (IFS) meteorological model through data assimilation (Hersbach et al., 2020). ERA5 is globally available at 0.25 ° × 0.25 ° (~31 km) resolution and at hourly resolution from 1979 to within 5 days of real-time. It has been widely used in current studies due to its strength in both coverage and accuracy. In this study, the location of ERA5 data is centered at latitude 1.4° and longitude 103.9°, corresponding to the closest point (about 18.32 km away from SDE2 building) to the site.

The ERA5 climate data downloaded in the present study is for the year 2019. The parameters we obtain from ERA5 are: 2 m air temperature, i.e., the dry bulb temperature; surface pressure, which represents the atmospheric pressure on the surface of land; 2 m dew point temperature, which is used to calculate relative humidity; 10 m u-component of wind, 10 m v-component of wind, which are used to calculate 10 m wind speed; surface solar radiation downwards and total sky direct solar radiation at the surface, which represent global solar radiation and direct horizontal radiation, respectively. They are used to calculate direct normal radiation and diffuse solar radiation.

In addition, the TMY-ERA5 dataset is used as a reference. This global typical meteorological year (TMY) dataset is created using the ERA5 data and the Chinese Standard Weather Database (CSWD) method to represent the average historical weather conditions (Wu et al., 2023).

2.3. Urban land surface models

In this study, we introduce two urban land surface models, Urban Tethys-Chloris (UT&C) and Urban Weather Generator (UWG), to generate bias-corrected ERA5 data. Table 2 shows the comparison between UT&C and UWG. UT&C excels in simulating detailed urban ecohydrological processes by coupling complex vegetation and soil models with urban canopy dynamics. UWG is suitable for generating urban weather data for energy and building performance studies using simplified vegetation and soil representations and rural weather input.

Table 2
Comparison between UT&C and UWG (Bueno et al., 2012; Lipson et al., 2023; Meili et al., 2020).

Aspect	UT&C	UWG
Purpose	Generate pedestrian-level weather data accounting for biophysical and eco-physiological information from weather data above urban canyon	Generate urban weather data accounting for urban heat island effects from rural weather data
Built complexity	Canyon (3 or 4 urban facets); two-layer atmosphere in urban canopy	Canyon (3 or 4 urban facets); multi-layer atmosphere in urban canopy
Hydrological complexity	Multi-layer soil hydrology; complex vegetation land surface model	Simplified vegetation & soil hydrology
Behavior complexity (anthropogenic heat and water flux)	Constant anthropogenic heat flux; dynamic irrigation (e.g., soil witness)	Building energy model (internal fluxes); dynamic irrigation

To obtain urban parameters, the surrounding area is selected as a region within a 200-meter radius circle centered at SDE2 building, based on a sensitivity analysis of the surrounding area's radius. The analysis demonstrates a slight sensitivity of air temperature to urban parameters collected from various surrounding area's radius, as detailed in Appendix A. The urban parameters used as inputs for the two models are given in Table 3.

Note that canyon orientation is a crucial input in urban land surface models (Zheng et al., 2023). In the present study, it is measured as the clockwise angle between a street's long axis and geographic north. For instance, an orientation of $\pi/2$ indicates a west-to-east street alignment.

2.3.1. Urban Tethys-Chloris model

Urban Tethys-Chloris (UT&C) model integrates principles of

Table 3
Urban parameters used in UT&C and UWG.

Parameter	Value
Building coverage ratio	0.25
Average building height (m)	22.5
Width of roof (m)	33.0
Canyon width (m)	99.0
Canyon orientation (°)	20
Tree crown radius (m)	8.0
Tree height (m)	13.25
Tree distance to wall (m)	13.0
Vegetated ground proportion	0.7
Impervious ground proportion	0.3

ecosystem modeling with urban canopy schemes to assess the impact of vegetation on urban climate and hydrology. It is based on the infinite urban canyon approximation to input the complex urban system (Meili et al., 2020). The model is designed to integrate urban geometry, energy budget, water budget, and vegetation processes into a cohesive model that can simulate the interactions between the urban environment and vegetation.

UT&C model incorporating parameters such as canyon height and width, building roof width, and ground surface types (impervious, bare soil, and vegetated). Street trees are represented by their height, canopy radius, and proximity to building walls. The energy budget is determined by modeling radiative transfer, turbulent fluxes, and conductive heat fluxes, accounting for shading, multiple reflections, and heat storage in urban materials. Turbulent fluxes (sensible and latent heat) use resistance-based methods to model aerodynamic interactions at various levels. The water budget tracks canopy interception, ponding, soil moisture dynamics, and runoff, with options to retain runoff or include irrigation inputs. Vegetation processes, including photosynthesis, stomatal behavior, and root water uptake, are modeled separately for sunlit and shaded canopy areas, considering root distribution and water interception, offering a detailed representation of urban-environment interactions (Meili et al., 2020).

The atmospheric forcing height, which is assumed to be 3 times the canyon roof height, serves as the input height for meteorological inputs in UT&C (Oke et al., 2017). In this study, the canyon height is set to 22.5 m and the forcing height is set to 67.5 m. It is worth noting that height-based corrections are required for all input parameters, as outlined in Appendix B.

2.3.2. Urban weather generator

Urban Weather Generator (UWG) is another widely used urban land surface model that can simulate the mean energy fluxes across the surface of a simplified homogenous urban morphology representing urban canyons (Bueno et al., 2012).

UWG consists of four interconnected sub-models: the Rural Station Model (RSM), Vertical Diffusion Model (VDM), Urban Boundary Layer Model (UBL), and Urban Canopy – Building Energy Model (UC-BEM) (Bueno et al., 2012). The RSM reads ERA5 weather data, calculates heat transfer between the atmosphere, ground soil, and vegetation, and provides this information to the VDM and UBL. The VDM then processes data to generate vertical air temperature profiles, incorporating heat fluxes from the RSM. Subsequently, the UBL simulates temperatures just above the urban canopy using these profiles and heat flux data from both the RSM and UC-BEM. Finally, the UC-BEM provides heat flux calculations to the UBL and outputs final urban meteorological parameters. Its building parametrization module provides information on heat transfer through windows, infiltration, and ventilation, among other factors, and facilitates the estimation of heating and cooling loads for urban blocks, which was developed based on the Town Energy Balance (TEB) model by Masson (Bueno, 2010; Masson et al., 2002). It also separates internal heat gains into convective, radiant, and latent components, simplifies heating and cooling load calculations, and estimates cooling demand (Bueno et al., 2012).

In this study, we consider ERA5 as rural data and use it as input for UWG to generate local weather data, which will be labeled as UWG-ERA5 throughout this article. Note that the input forcing height of UWG is the same as that of ERA5. Therefore, no height-based corrections need to be made. The temperature and humidity of the output data can represent the values at 2 m, and the output wind speed at 10 m (Bueno et al., 2012).

2.4. Building energy modeling

The open-source building energy simulation program, EnergyPlus, is employed in the present study. EnergyPlus combines various building system modules to reproduce thermal zones using heat balance models (Crawley et al., 2001). We categorize different zones based on their actual functions and locations within SDE2 building. Details of the building energy model are described in the following subsections:

2.4.1. Building geometry and thermal zones

Fig. 3(a) shows the models of SDE2 building created in EnergyPlus to represent floors, envelopes, windows, and external shadings. The building is divided into 58 zones, including 23 air-conditioned zones and 35 non-air-conditioned zones (Fig. 3(b)). Following the actual condition, computer laboratories, classrooms, shared offices, private offices, and indoor corridors with air conditioners (AC) are regarded as air-conditioned zones. All other areas, where air conditioners are not equipped or not in operation, are classified as non-air-conditioned zones.

2.4.2. Model calibration

In building energy simulations, it is common for certain parameters that impact building energy demand to either be uncertain or unavailable. Calibration helps to adjust these unknowns, enhancing the reliability of the simulations and ensuring a closer alignment with actual conditions. In the present study, some of the building parameters are based on the actual situation of SDE2 building. However, other unknown parameters, including cooling setpoints, infiltration rate, and the operating schedule on weekdays, weekends, and holidays, are chosen for calibration.

A genetic algorithm is used to calibrate the unknown parameters by Galapagos, a Grasshopper-based plugin Rutten (2013). The meter data of hourly building cooling load, which was read from the electricity meter, is available from Feb 1 to Sept 27, during which the data from July 11 to July 17 is not used for calibration due to a technical error. The calibration refers to the criteria of ASHRAE standard to evaluate and minimize the model uncertainties.

All the unknown parameters are set as the target parameters for the optimization. Throughout the calibration process, the metered cooling load is fed into the genetic algorithm-based model. The locally measured weather data is input to EnergyPlus, and the output generated by each iteration of the algorithm is then compared with the measured meter data. The deviation between the model's output and the actual measured data is quantified using the Coefficient of Variation of Root-Mean-Square Error (CV(RMSE)), as defined in Eq. (1). The optimization process is to identify the combination of unknown parameters that yields a stable and qualified result of CV(RMSE). Following the model's initial fulfillment of the hourly CV(RMSE) criterion according to ASHRAE Guideline 14 (ASHRAE, 2014), the optimization process underwent several additional iterations. Since Normalized Mean Bias Error (NMBE) is a widely recognized criterion for assessing the calibration success of BEM (Chong et al., 2021), the NMBE is also included here, as referenced in Eq. (2).

$$CV(RMSE)\ (\%) = \left(\frac{1}{\overline{m}}\right) * \sqrt{\frac{\sum_{i=1}^{n}(m_i - s_i)^2}{(n - p)}} * 100 \quad (1)$$

$$NMBE\ (\%) = \left(\frac{1}{\overline{m}}\right) * \frac{\sum_{i=1}^{n}(m_i - s_i)}{(n - p)} * 100 \quad (2)$$

where m_i and s_i are the measured and simulated values respectively, $\overline{m}$ is the averaged measured values, n is the number of data points, and p is the number of parameters. In the present study, only one parameter, i.e. building cooling load, is evaluated. Therefore, p equals 1 (ASHRAE, 2014). The resulted NMBE and CV(RMSE)) are 3.26 % and 29.24 %, respectively. According to ASHRAE Guideline 14, hourly criteria of NMBE below 10 % and CV(RMSE) below 30 % indicate a good model fit with acceptable predictive capabilities (ASHRAE, 2014).

The two performance indices defined in Eqs. (1) and (2) are consistently used for the evaluation of BEM results in SubSection 3.3.

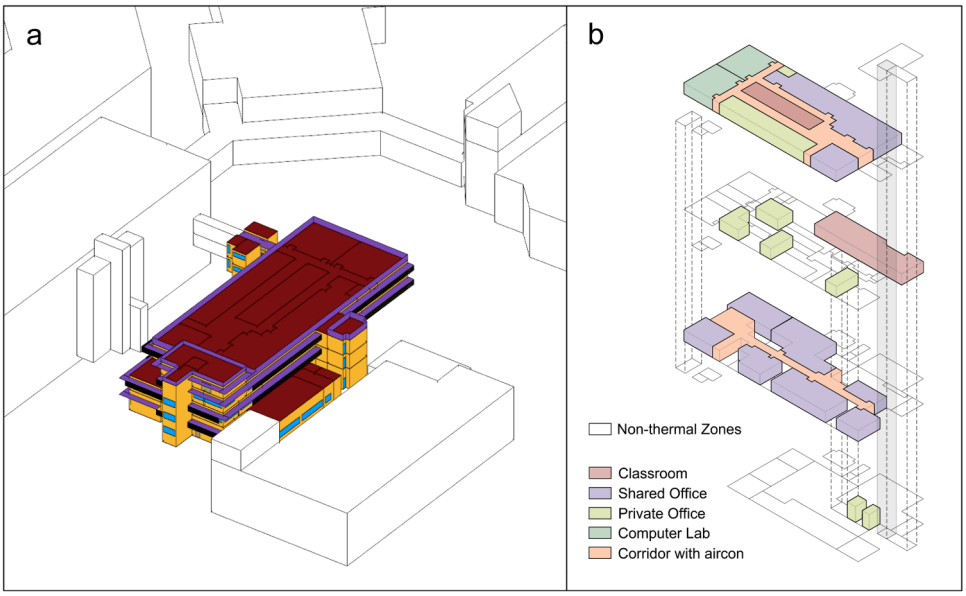

Fig. 3. Model of SDE2 building in EnergyPlus: (a) building geometry; (b) isometric view of air-conditioned zones and non-air-conditioned zones.

2.5. Metrics for the evaluation of weather data

In the present study, Mean Absolute Error (MAE) and Root Mean Square Error (RMSE) are employed to evaluate the goodness of fit for weather data. MAE measures the average absolute error, reflecting the typical deviation from the Local dataset, while RMSE, by squaring errors before averaging and taking the square root, emphasizes larger deviations, which are critical for applications sensitive to extreme temperature errors. MAE and RMSE are expressed in Eqs. (3) and (4):

$$MAE = \left(\frac{1}{m}\right) * \sum_{i=1}^{m} |F_i - O_i| \tag{3}$$

$$RMSE = \sqrt{\frac{\sum_{i=1}^{m} (F_i - O_i)^2}{m}} \tag{4}$$

where m is the number of observations, F_i and O_i are forecasted and observed values of the i_{th} *day*, respectively. To ensure the comparability of all datasets, height-based corrections will be done by the method shown in Appendix B.

3. Results

3.1. Meteorological parameters

In this study, we analyze weather datasets used for Building Energy Modeling (BEM) from February to December 2019, a period for which local meteorological data is available. Datasets being compared include ERA5, TMY-IWEC, TMY-ERA5, UT&C-ERA5, and UWG-ERA5, all benchmarked against the locally measured meteorological data. The meteorological parameters examined in this comparison are dry bulb temperature, relative humidity, wind speed, and solar radiation.

3.1.1. Dry bulb temperature

Fig. 4(a) depicts dry bulb temperature averaged for each hour across all days from February to December 2019. The locally measured temperature (Local) exhibits more pronounced diurnal fluctuations with approximately 5 °C difference and records the highest peak temperature of 31.23 °C among all datasets at 13:00. UT&C-ERA5 and TMY-IWEC show a relatively closer alignment with Local, particularly in terms of the time and magnitude of the peak temperature. ERA5, UWG-ERA5, and TMY-ERA5 datasets exhibit a minimal diurnal temperature range, which is <1.3 °C. UWG-ERA5, which accounts for the impact of the UHI effect, exhibits an overall higher temperature compared to ERA5 while preserving a similarly moderate daily fluctuation pattern. Fig. 4(b) demonstrates the monthly average temperature during the study period. As observed for the daytime dry bulb temperature, the results for the monthly average temperature are lower than the Local dataset in almost all cases. Moreover, the results highlight that UWG can significantly increase the monthly average temperature compared to the original ERA5, and aligns marginally better with the Local. Nevertheless, the UT&C-ERA5 exhibits lower average temperatures, largely due to the decrease in nighttime temperatures, than the original ERA5.

Fig. 4(c) and (d) show the MAE and RMSE results of diurnal variations of all datasets compared to Local, which are calculated based on the hourly data from February to December 2019 using Eqs. (3) and (4). Overall, the trend of MAE and RMSE of different datasets are consistent. The result highlights that the UT&C-ERA5 outperforms the other datasets and suggests that morphing by UT&C has enhanced the accuracy of ERA5 weather data at the study area, while the improvement by UWG is minimal.

Fig. 4(e) displays the hourly results of all the datasets in March, the hottest month according to the data from the weather station near SDE2 building during the study period. It is observed that UT&C model can significantly improve the ERA5's alignment with Local by correcting the overall bias in the peak value in the original ERA5 data. In contrast, UWG-ERA5 shows minimal changes in the diurnal temperature trend compared to ERA5, except for a slight overall increase. The results indicate that TMY-IWEC, despite showing a good fit in Fig. 4a, fails to follow the general temperature trends measured in March 2019. This discrepancy is due to the nature of TMY data, which is compiled from different months across past years, leading to frequent anomalies. These irregularities contribute to the higher MAE and RMSE values observed, which are not reflected in Fig. 4a.

3.1.2. Relative humidity

Fig. 5(a) illustrates the relative humidity averaged for each hour across all days. Local data shows similar fluctuations compared to dry bulb temperature, with approximately 21 % difference between daytime and nighttime, which is also observed for UT&C-ERA5 and TMY-IWEC. On the other hand, ERA5, UWG-ERA5, and TMY-ERA5 only have approximately 5 % differences. Besides, UWG also decreased all the

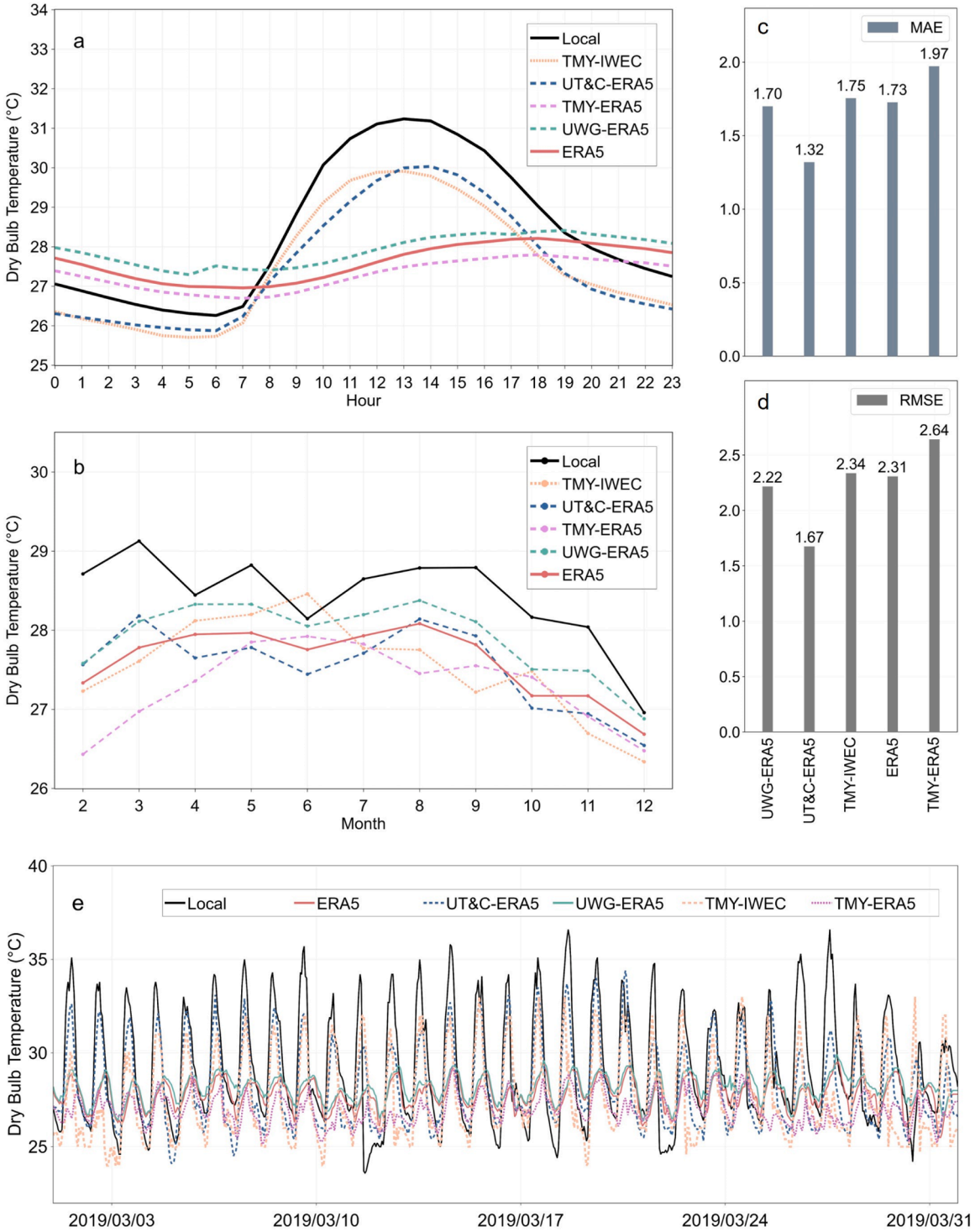

Fig. 4. Dry bulb temperature (a) averaged for each hour across the entire study period; (b) averaged for each month across the entire study period; (c) MAE; (d) RMSE; (e) hourly data in March 2019.

hourly values in the diurnal cycle. Fig. 5(b) demonstrates the monthly average relative humidity. The UT&C-ERA5 shows a significant increase in relative humidity compared to the original values in the ERA5 data, while UWG-ERA5 demonstrates a consistent, marginally lower trend each month compared to ERA5.

Fig. 5(c) and (d) show the MAE and RMSE results of all datasets compared to Local. Results suggest the overall improvement of UT&C-ERA5 is not significant, with a reduction of 0.32 in MAE and 0.22 in RMSE, and UWG-ERA5 shows an even worse performance on relative humidity. MAE and RMSE results are generally consistent across the weather data, except TMY-IWEC that yields a slightly higher error in RMSE. Fig. 5(e) reveals the hourly results of all the datasets in March. It is observed that both UT&C-ERA5 and TMY-IWEC significantly overestimate the humidity for over 15 days in this month, and UWG-ERA5 is slightly lower than the original ERA5.

3.1.3. Wind speed

Fig. 6(a) illustrates hourly-averaged diurnal variations of wind speed

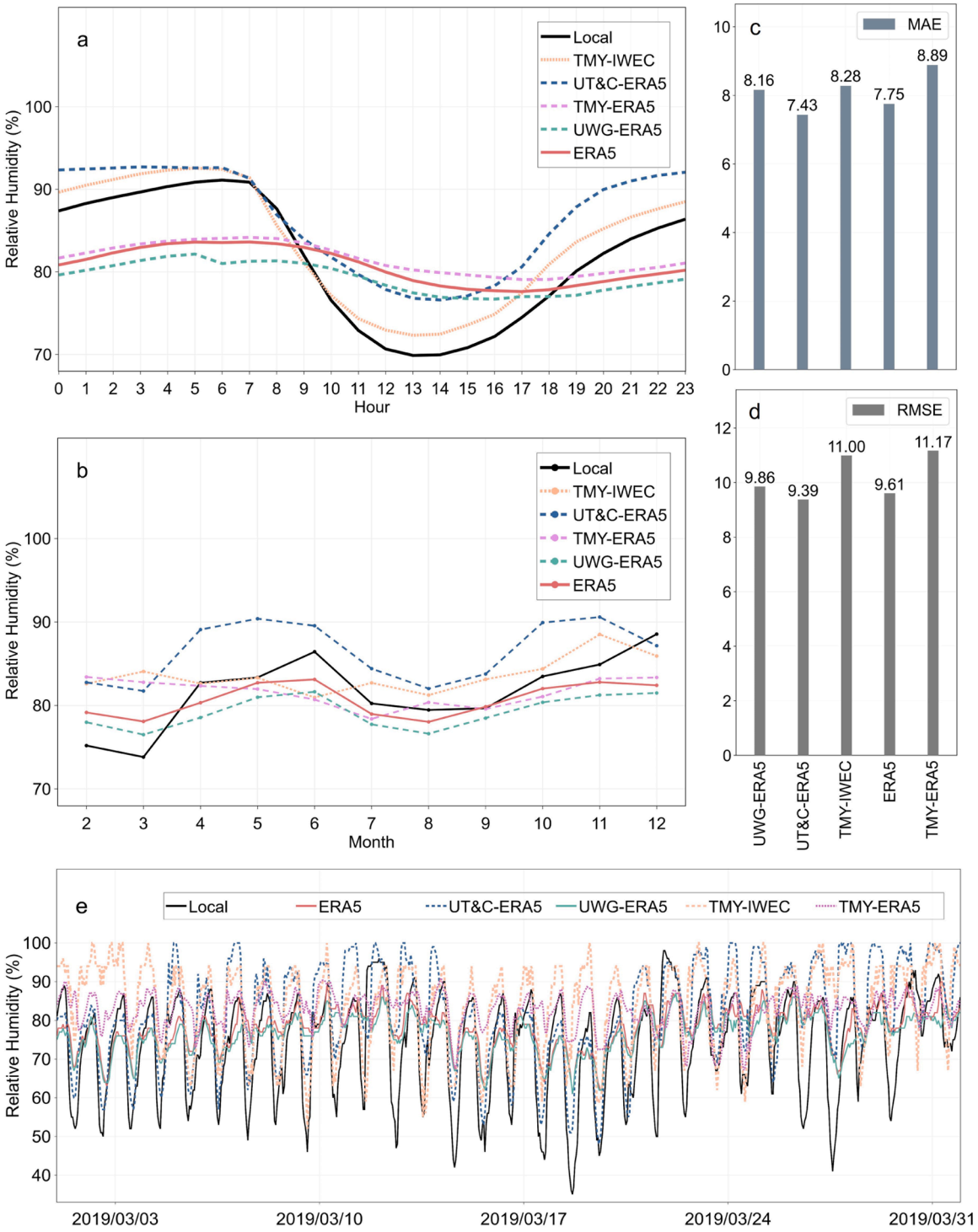

Fig. 5. Relative humidity (a) averaged for each hour across the entire study period; (b) averaged for each month across the entire study period; (c) MAE; (d) RMSE; (e) hourly data in March 2019.

at 10 m above ground level. ERA5 and UT&C-ERA5 are shown together because UWG maintains the input wind speed of ERA5 unchanged since it assumes the wind speed input at the rural station (ERA5 in this study) is equal to that above the urban canopy (Bueno et al., 2012). It is revealed that overestimation exists in all the datasets compared with Local. Among them, TMY-ERA5 shows the highest overestimation, peaking at 3.84 m/s compared to 1.15 m/s for Local. In the afternoon, ERA5 and UT&C-ERA5 exhibit opposite trends in variation. A similar anomaly is also found in the wind speed of ERA5 datasets in a previous study (Dai, 2023), showing a drop in the daytime. The oceanic climate in Singapore is a possible factor to cause this tendency observed in ERA5 (Dai, 2023). TMY-IWEC, though having the same trend as Local, is observed to have a surge during peak hours that does not exist in the others. Fig. 6(b) shows the monthly average wind speed. It is observed that UT&C-ERA5 and TMY-IWEC align better with Local than other datasets, despite their overestimations of the diurnal variation.

Fig. 6(c) and (d) indicate that UT&C-ERA5 performs better than the others in terms of MAE and RMSE. The MAE result of TMY-IWEC is

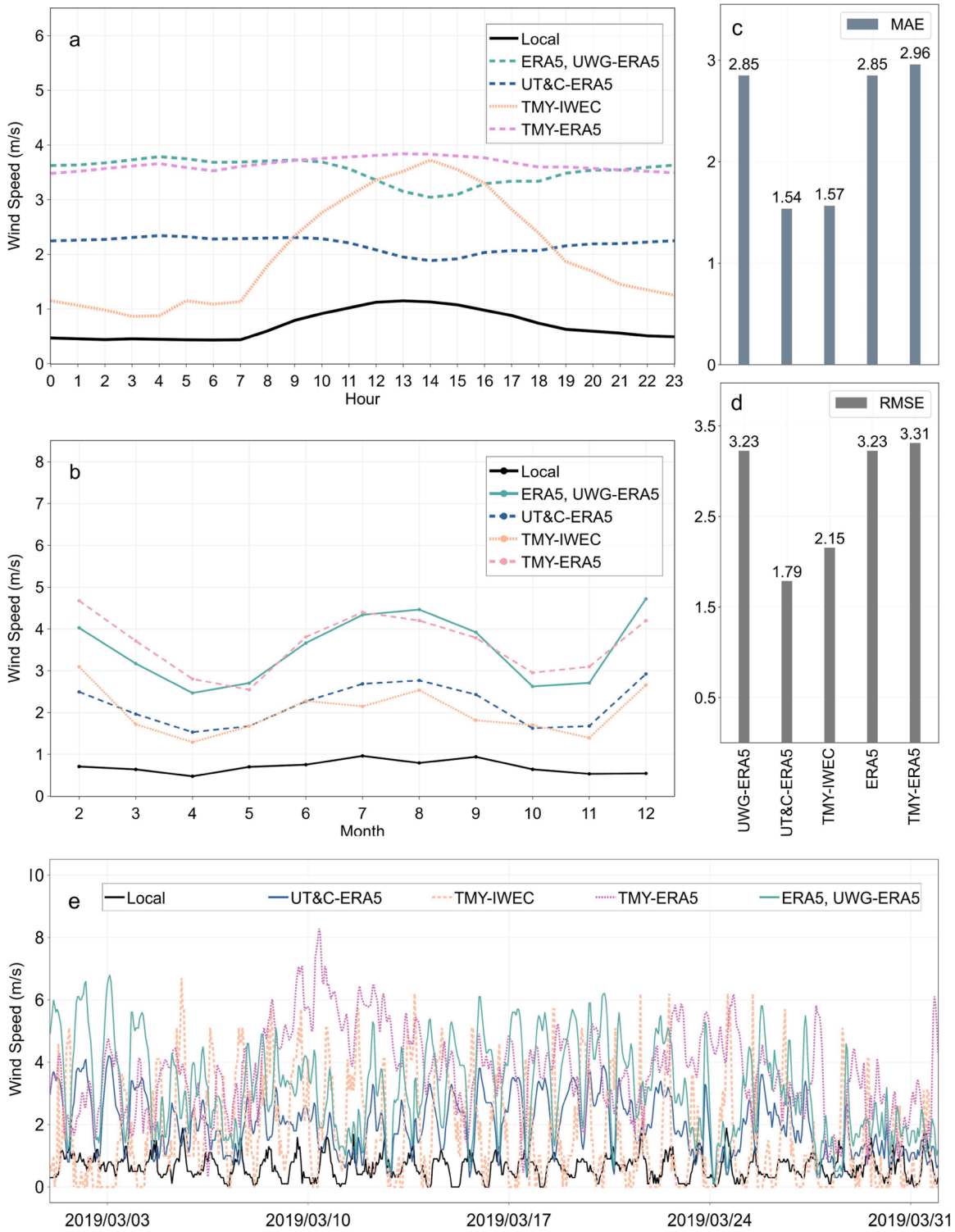

Fig. 6. Wind speed (a) averaged for each hour across the entire study period; (b) averaged for each month across the entire study period; (c) MAE; (d) RMSE; (e) hourly data in March 2019.

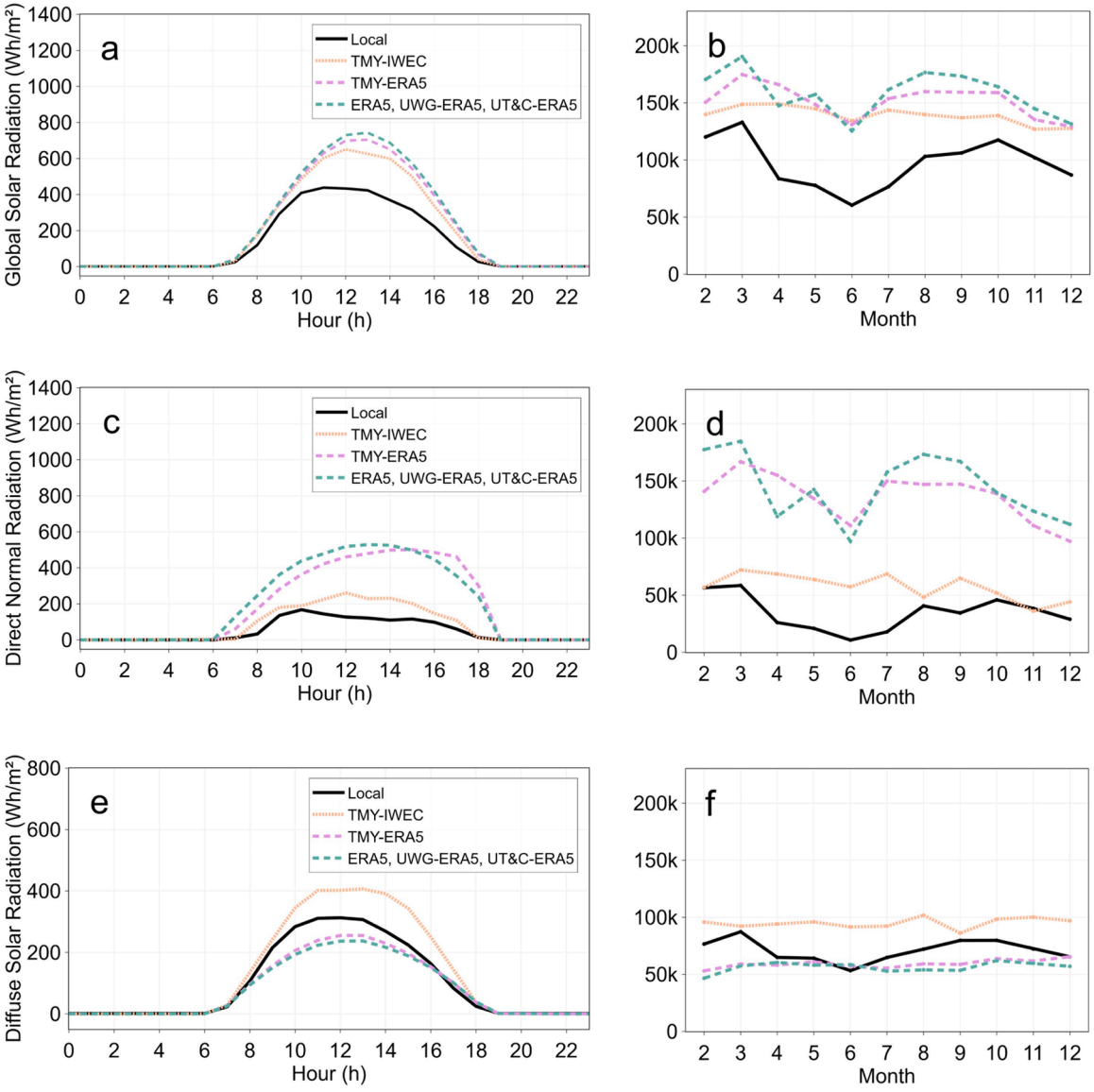

Fig. 7. (a) Global solar radiation averaged for each hour across all days and (b) total monthly radiation in the entire study period; (c-d) same for direct normal radiation; (e-f) same for diffuse solar radiation.

similar to UT&C-ERA5, while the RMSE result of TMY-IWEC is slightly higher. This also indicates that the wind speed fluctuation during daytime is the most significant in TMY-IWEC. Furthermore, Fig. 6(e) provides the hourly variation of wind speed in March 2019, which also shows that the UT&C model reduced the deviation between ERA5 and Local.

3.1.4. Solar radiation

Global solar radiation, direct normal radiation, and diffuse solar radiation are inputs for building energy modeling. Notably, all the radiation parameters of ERA5 are not morphed by UT&C or UWG.

Fig. 7 depicts the global solar radiation, direct normal radiation, and diffuse solar radiation of hourly averaged diurnal variation and total monthly variation. Fig. 7 (a-b) indicates that all the datasets yield a higher global solar radiation than the Local. Among them, TMY-IWEC shows a relatively small deviation from the Local dataset, whereas ERA5 exhibits the largest discrepancies. Fig. 7 (c-d) shows the results of direct normal radiation. ERA5 has a peak value of 529 Wh/m^2, which is approximately 3 times that of Local. TMY-ERA5 shows a similar result. In contrast, ERA5 and TMY-ERA5 provide lower diffuse solar radiation than Local, as shown in Fig. 7 (e-f).

3.2. Cooling degree days

Degree days is an indicator that is commonly used in the analysis of building energy demand (De Rosa et al., 2014). Heating degree days (HDD) and cooling degree days (CDD) can be proxies of the estimations of heating and cooling load in buildings located in certain climate conditions. In the present research, CDD in the study period is calculated by:

$$CDD = \sum_{i=1}^{334} \max(0,\ T_{m,i} - T_c) \tag{5}$$

where i is the i_{th} day of the study period, and $T_{m,i}$ is the daily mean air temperature on i_{th} day; T_c, the cooling base temperature takes 24 °C, which is the usual base temperature in Singapore (Singapore Productivity & Standards Board, 2024).

Fig. 8 plots the CDD on each day based on all these datasets in the study period. The results of MAE and RMSE are consistent. It is obvious that all the selected datasets tend to underestimate CDD values on most

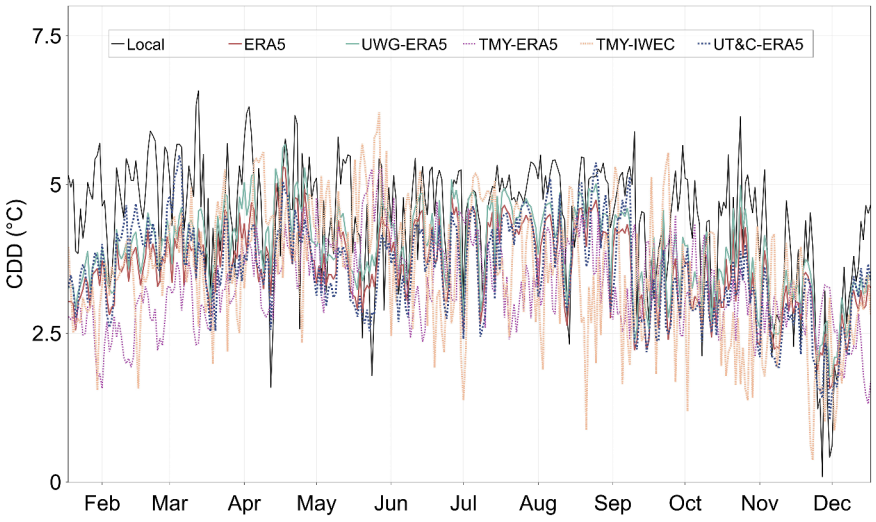

Fig. 8. Hourly CDD of all datasets compared with Local across the entire study period.

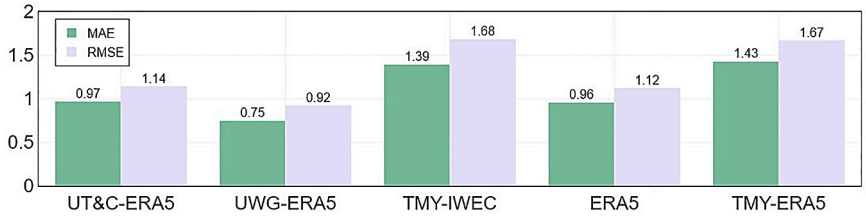

Fig. 9. MAE and RMSE of CDD of all datasets compared to Local during the entire study period.

days. Fig. 9 displays error metrics, indicating that UWG-ERA5 fits the best with Local in terms of both MAE and RMSE. UT&C-ERA5, despite having a better performance than the original ERA5, provides a worse alignment with the benchmark data in CDD.

3.3. Hourly cooling load

The weather datasets are then used as inputs in the calibrated building energy model to estimate the building cooling load for the SDE2 building. The simulation period is 11 months, from February to December. As mentioned in SubSection 2.4.2, NMBE and CV(RMSE) defined in Eqs. (1) and (2), are consistently used here. Note that the simulated building cooling load with the local weather data is considered as the benchmark for comparative analysis. The hourly building cooling load obtained from the other five weather datasets are compared with this benchmark.

Fig. 10(a) displays the simulation result of the cooling load averaged in one week across all 334 days. UT&C-ERA5 overestimates cooling loads, mainly during the peak hours of each day, while the others underestimate the cooling load on both weekdays and weekends. Meanwhile, UWG-ERA5 demonstrates a slightly higher cooling load than ERA5. Fig. 10(b) shows the simulated hourly cooling load in March. It indicates that the two urban land surface models perform differently during peak hours. UT&C-ERA5 demonstrates a better alignment with Local despite overestimation on several days in March. The underestimation in TMY-ERA5 during peak hours is significant, and TMY-IWEC has relatively less deviations from Local. However, TMY-IWEC demonstrates frequent anomalies. Like the results observed in dry bulb temperature, these anomalies also exist in the hourly cooling load data.

Fig. 11 shows simulated hourly peak cooling loads on each day over the study period for all the datasets and their MAE and RMSE compared to Local data in March 2019. It is indicated that generally, UT&C-ERA5 slightly overestimates the peak cooling load, while ERA5, UWG-ERA5, and TMY-ERA5 underestimate the peak cooling load. Among the datasets, UT&C-ERA5 closely aligns with Local data during the entire study period, having the lowest deviation (MAE: 12.07, RMSE: 16.19), as shown in Fig. 12. The results of the peak cooling load align with the findings in the simulated hourly cooling load. The possible reason is that UT&C model corrects the overall bias of ERA5 in the peak temperature, as detailed in 3.1.1. In addition, the two TMY datasets both show high biases in peak cooling load. Compared with Local, the deviation of TMY-IWEC fluctuates significantly, and TMY-ERA5 generally indicates the greatest underestimation in peak cooling load among all the datasets.

Fig. 13 presents the NMBE and CV(RMSE) values for hourly cooling load predictions of SDE2 building using the five weather datasets. Results of UT&C-ERA5 show an overestimation while the others underestimate the cooling load. Compared to the original ERA5, both UT&C-ERA5 and UWG-ERA5 yield results with better agreement with Local.

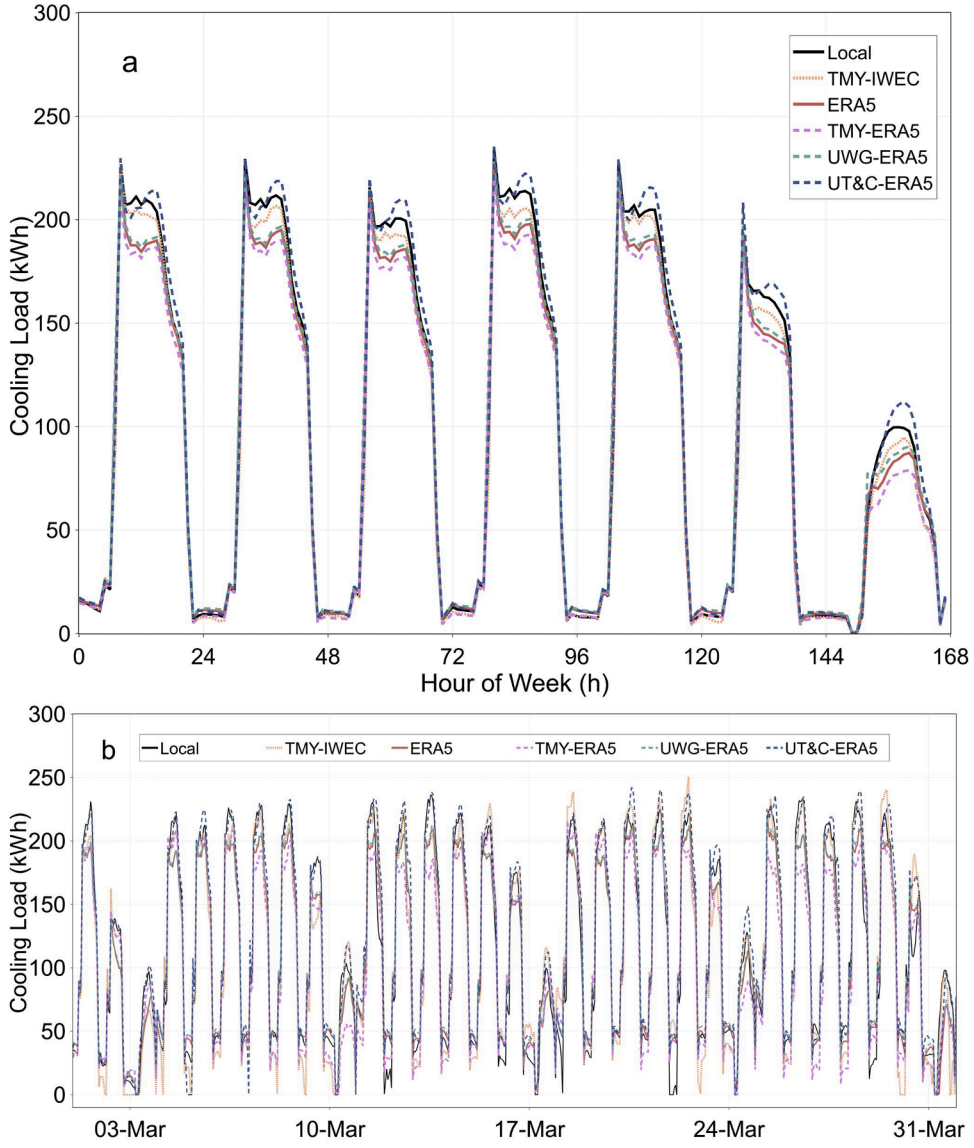

Fig. 10. Simulated hourly cooling load (a) in an ideal week averaged across all days in the entire study period; (b) in March 2019.

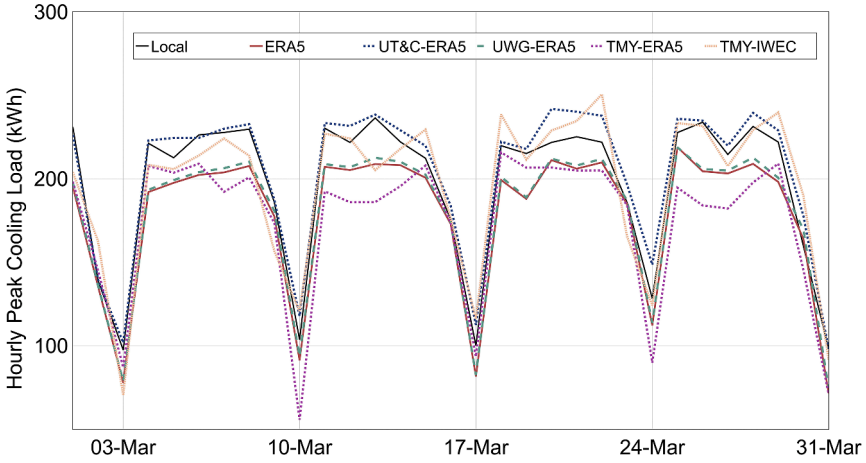

Fig. 11. Simulated hourly peak cooling load on each day during March 2019.

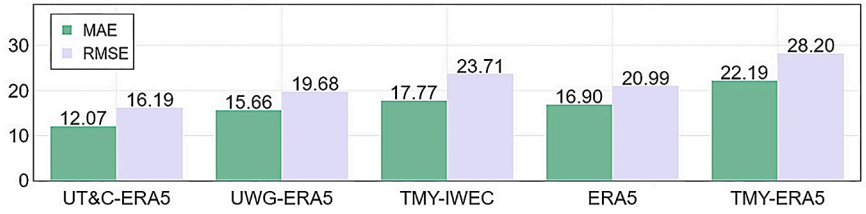

Fig. 12. MAE and RMSE of the simulated hourly peak cooling load on each day during the entire study period using the five datasets.

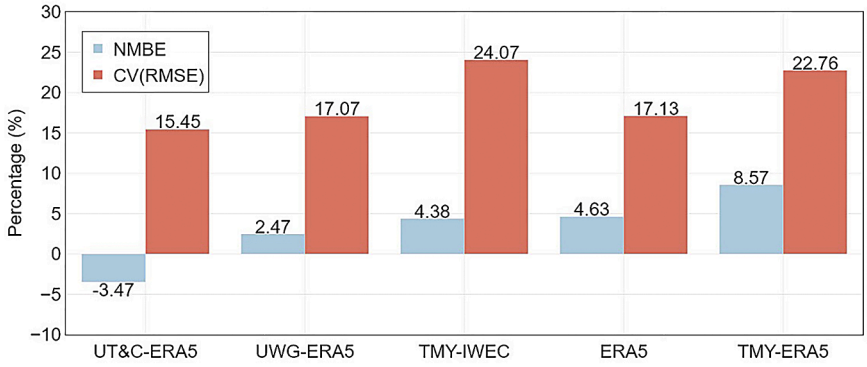

Fig. 13. NMBE and CV(RMSE) of simulated hourly cooling load using all the datasets compared to Local during the entire study period.

Notably, UWG-ERA5 achieves the lowest NMBE, whereas UT&C-ERA5 exhibits the lowest CV(RMSE). These findings suggest that enhancing weather data through urban land surface models improves the accuracy of building cooling load predictions in BEM, outperforming predictions based on the unmodified ERA5 dataset. Notably, TMY-IWEC performs well in NMBE but shows the highest CV(RMSE) result due to its significant deviation observed in peak cooling load simulation. The statistical treatment in Appendix C further discusses the outliers of TMY-IWEC and its impact on the result of error metrics.

4. Discussion

4.1. Performance of selected weather data

Overall, the results of UT&C-ERA5 and UWG-ERA5 indicate an improvement in meteorological parameters by the urban land surface models. However, parameters of canyon geometries and vegetation properties are crucial inputs for UT&C and UWG. The underestimation of daytime temperature by ERA5 may be due to its deficiency in reproducing high temperatures in coastal cities (Zou et al., 2022), while urban land surface models can correct the heat storage within urban canyons. Meanwhile, vegetation settings and ground surface fractions can have a significant impact on the proportion of sensible heat flux and latent heat flux (Meili et al., 2020), leading to a drop in nighttime temperature in UT&C output. The effects of UT&C and UWG on the meteorological parameters of ERA5 differ significantly, despite improvements achieved by both urban land surface models. Overall, UT&C-ERA5 demonstrates greater fluctuations and more accurate peak values compared to UWG-ERA5, reflecting the differing physical mechanisms underlying the two models. UWG assumes that the urban boundary layer is a region of well-mixed air with no significant heat exchange at the top (Bueno et al., 2012). It solves an energy balance for a control volume with imposed boundary conditions by arbitrarily assigning different default thicknesses for the layer during the day and night (Afshari, 2023). UT&C implements a sophisticated and robust urban vegetation process, with a comprehensive consideration of the water budget (Meili et al., 2020). In comparison, TMY-ERA5 has the largest errors compared to Local, and TMY-IWEC shows inconsistency in the results of MAE and RMSE in relative humidity, wind speed, and simulated hourly cooling load. The discrepancy is due to the nature of TMY data, which is compiled from different months across past years, leading to frequent anomalies in hourly data.

4.2. The use of CDD on the estimation of cooling load

Unlike dry bulb temperature and hourly building cooling load, the CDD of UT&C-ERA5 fails to deliver an improvement compared to ERA5. The major limitation of CDD is using daily mean temperature for rough estimation, which fails to capture detailed energy demand patterns, including peak cooling load and daily fluctuations. Studies indicate that relying solely on daily mean air temperature might overestimate or underestimate the mean values based on regional climate (Tsonis et al., 2019). Moreover, CDD does not account for factors like humidity, wind speed, solar radiation, building characteristics, or other factors (Al-Hadhrami, 2013; De Rosa et al., 2014). These omissions can result in significant inaccuracies and lead to a coarse result when estimating cooling load.

4.3. Limitations

Several limitations of this study are outlined to guide future research efforts. First, as the building environment and building thermal energy consumption are responsive to the solar radiation conditions, solar radiation plays a key role in building energy consumption (Causone et al., 2010). Second, the two selected urban land surface models fail to correct the deviations in ERA5 solar radiation data. In the present study, the shading geometries (shades, shutters, and surrounding buildings) were built in BEM to better reflect the impact of solar radiation on building cooling load. Recent studies have developed methods for predicting surface radiation in the urban context (Anselmo et al., 2024; Desthieux et al., 2023). Future need for solar radiation adjustments in urban land surface models should be emphasized. Third, both models assume a canyon urban morphology, characterized by infinite rows of buildings, which may limit their accuracy in representing complex urban environments. Further investigations using urban land surface models with block array (e.g., canopy model (Kondo et al., 2005)) or resolved building (e.g., microscale urban surface energy model (Lee & Lee, 2020)) geometries can be conducted in the future. Fourth, while this study focuses on a single building in Singapore, future research should aim to assess the proposed method across diverse tropical urban settings, considering different urban densities and building types to test its generalizability and robustness beyond the immediate study area. Lastly, since this study focuses solely on one area, future investigations should explore a broader range of climates within tropical regions.

5. Conclusion

This study explores different approaches to generate local weather data using urban land surface models for building energy simulation. ERA5 reanalysis data is adopted as input and processed by two urban land surface models, i.e., Urban Tethys-Chloris (UT&C) and the Urban Weather Generator (UWG). Subsequently, the local weather datasets are used for building energy modeling to determine the cooling load of a multi-story educational building in Singapore. The results are benchmarked with the simulated building cooling load using the locally measured weather data. It is concluded that:

- The two generated local weather data by UT&C model and UWG model, namely, UT&C-ERA5 and UWG-ERA5, respectively, demonstrate enhancement in the hourly local weather data over the original ERA5. For dry bulb temperature, UT&C reduces MAE from 1.73 to 1.32 and RMSE from 2.31 to 1.67. This improvement corrects the smaller diurnal temperature range of the original ERA5 data. While UWG shows a smaller reduction from 1.73 to 1.70 in MAE, and from 2.31 to 2.22 in RMSE. Besides, all the datasets overestimate the local wind speed. Among them, UT&C-ERA5 achieves a better accuracy in wind speed with a reduction in MAE from 2.85 to 1.54 and RMSE from 3.23 to 1.79 compared to the original ERA5. The two TMY datasets are generally less accurate. TMY-IWEC shows relatively good alignment with local data in terms of wind speed and solar radiation, and also demonstrates results with a stable overall accuracy in simulated cooling load results averaged for each hour in the entire study period. However, it exhibits obvious deviations in the hourly meteorological parameters overall and shows more frequent anomalies.
- Building energy modeling (BEM) with two datasets generated by urban land surface models shows an improved prediction of hourly building cooling load compared to the original ERA5. UT&C-ERA5 reduces CV(RMSE) from 17.13 % to 15.45 %, and NMBE from 4.63 % to −3.47 %, while UWG-ERA5 reduces CV(RMSE) from 17.13 % to 17.07 %, and NMBE from 4.63 % to 2.47 %. UT&C-ERA5 and UWG-ERA5 also achieve good performance in simulated peak cooling loads.

This work highlights that the reanalysis-data-based approach can provide valuable data morphing for building energy simulation in tropical cities.

CRediT authorship contribution statement

Xing Zheng: Writing – review & editing, Writing – original draft, Visualization, Validation, Supervision, Software, Resources, Project administration, Methodology, Investigation, Funding acquisition, Formal analysis, Data curation, Conceptualization. **Naika Meili:** Writing – review & editing, Validation, Methodology. **Shuyang Li:** Data curation. **Huanhuan Wang:** Data curation. **Lei Xu:** Writing – review & editing. **Zhen Han:** Methodology, Writing – review & editing. **Martín Mosteiro-Romero:** Writing – review & editing, Methodology. **Yi Wu:** Methodology. **Da Yan:** Writing – review & editing, Data curation. **Dengkai Chi:** Data curation. **Guanli Feng:** Writing – review & editing, Writing – original draft, Visualization, Validation, Software, Methodology, Formal analysis, Data curation. **Rudi Stouffs:** Writing – review & editing, Supervision, Funding acquisition.

Declaration of competing interest

The authors declare that they have no known competing financial interests or personal relationships that could have appeared to influence the work reported in this paper.

Acknowledgment

The research was conducted partly at the Future Cities Lab Global at the Singapore-ETH Centre, which was established collaboratively between ETH Zurich and the National Research Foundation Singapore. This research is supported by the National Research Foundation Singapore (NRF) under its Campus for Research Excellence and Technological Enterprise (CREATE) programme. The authors would like to express sincere gratitude to Marcel Ignatius, Nyuk Hien Wong, Adrian Chong, Chao Yuan, and Liqing Zhang for their help in the data acquisition. Xing Zheng acknowledge a grant from City University of Hong Kong (Project No. (9610684)) for partially supporting the research in this paper.

Appendix A. Sensitivity analysis of the area of adjacent areas

The size of the adjacent areas of SDE2 building is the key factor in determining urban parameters. By selecting different areas as the site area, distinct changes are observed in urban geometries, vegetated and impervious ground proportions, and tree characteristics. These changes, in turn, influence the outcomes of urban climate models. Fig. A1 shows the 4 scenarios of sensitivity analysis conducted on the data morphing process, revealing significant variability in urban parameters when the site area is altered with different radii (200 m, 300 m, 400 m, and 500 m).

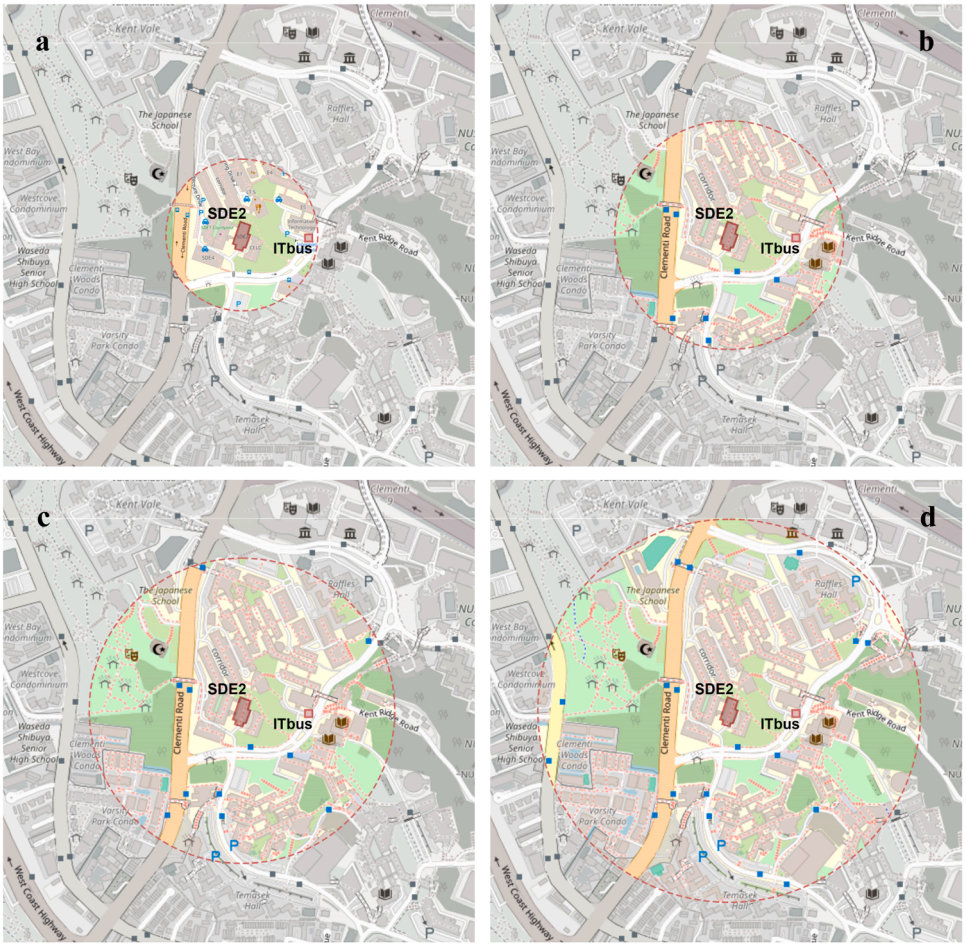

Fig. A1. The site areas that have been selected for sensitive analysis (a) 200 m radius (used for urban land surface models and energy simulation) (b) 300 m radius (c) 400 m radius (d) 500 m radius.

In the analyzed scenarios, increasing the radius led to variations in coverage ratio, average building height, and canyon width, highlighting the diverse urban fabric within each selected radius. At the SDE2 building site, a larger radius corresponded to an increase in vegetated ground proportion and a decrease in impervious ground proportion, indicating more green spaces in larger areas. Tree parameters such as crown radius, height, and distance from walls also showed differences. The urban parameters in different scenarios are listed in Table A1.

Table A1
Urban parameters used in different scenarios.

Geometric Parameters	Scenario 1: 200 m radius	Scenario 2: 300 m radius	Scenario 3: 400 m radius	Scenario 4: 500 m radius
Coverage Ratio	0.25	0.28	0.24	0.29
Average Building Height (m)	21.25	22.5	22.5	21.25
Width of Roof (m)	33.0	33.0	33.0	33.0
Canyon Width (m)	99.0	84.8	104.5	80.8
Canyon Orientation (°)	20	20	20	20
Tree Crown Radius (m)	8.0	10.0	10.0	10
Tree Height (m)	13.25	11.25	12.0	11.25
Tree Distance to Wall (m)	13.0	25.0	25.0	25.0
Ground Surface Fractions				
Vegetated Ground Proportion	0.7	0.8	0.85	0.9
Impervious Ground Proportion	0.3	0.2	0.15	0.1

The results in Fig. A2 indicate that urban green space of the periphery of SDE2 building is increasing with the larger site radius in this study, which slightly influenced the output dry bulb temperature during daytime. To balance the need for accurate simulation results with the computational time, this study selects the area of 200-meter radius scenario as the study area to better reflect the actual land surface parameters.

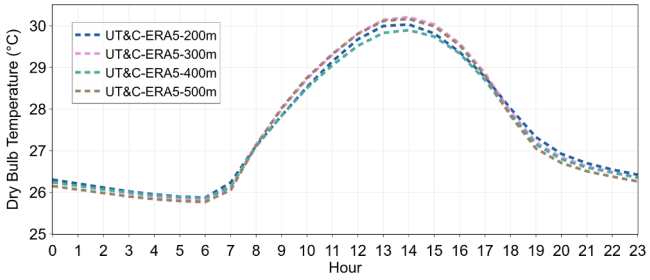

Fig. A2. Dry bulb temperature averaged for each hour of UT&C-ERA5 in scenarios with different radii across all days in the study period.

Appendix B. Height-based corrections of meteorological parameters

For all the datasets with incorrect height information as the forcing data of urban land surface models, or different from the uniform height for meteorological data comparison, corrections are undertaken. The methods for different meteorological parameters are:

(1) Dry Bulb Temperature: the known temperature at a certain height is used to obtain air temperature at the forcing height by Eq.(B1) assuming an environmental lapse rate (Γ) of -6.5 K·km^{-1} (Tang et al., 2021):

$$T_F = T + \Delta Z_{net}\Gamma \tag{B1}$$

where T_F is the dry bulb temperature at the forcing height, T is the known dry bulb temperature at a certain height, ΔZ_{net} is the height difference.

(2) Atmospheric pressure at the forcing height (p_F) is obtained using the hypsometric equation (Spiridonov & Ćurić, 2021):

$$p_F = p^* \exp\left(-\frac{g\Delta Z_{net}}{\overline{T}R_d}\right) \tag{B2}$$

where p is the known atmospheric pressure at a certain height, $g = 9.8$ m·s^{-2} is gravity acceleration, $\overline{T}$ is the middle temperature of the known height and the forcing height. In the present study, it is assumed as the mean value of T_F and T. $R_d = 287.05$ J·kg^{-1}·K^{-1} is the specific gas constant for dry air.

(3) Wind speed is determined using the log-law (Richards & Hoxey, 1993) assuming neutral stability and ignoring u^* (friction velocity, calculated based on hourly wind speed) differences:

$$U = \frac{u^*}{K}\ln\left(\frac{z + z_0}{z_0}\right) \tag{B3}$$

where U is the wind speed at the forcing height, $K = 0.41$ is von Karman's constant, z is the forcing height, z_0 is the surface roughness length. The data are assumed to represent short vegetation ($z_0 = 0.3$ m), but this might not accurately represent the actual urban scenarios (Tang et al., 2021).

(4) Relative humidity is assumed to stay constant with height to avoid supersaturation (Kokkonen et al., 2018).

Appendix C. Statistical treatment of TMY datasets

TMY datasets reportedly include anomalies in hourly profiles. The results have shown conflicts between different error metrics. Therefore, the outliers of all datasets in meteorological parameters and simulated cooling load are identified and assessed.

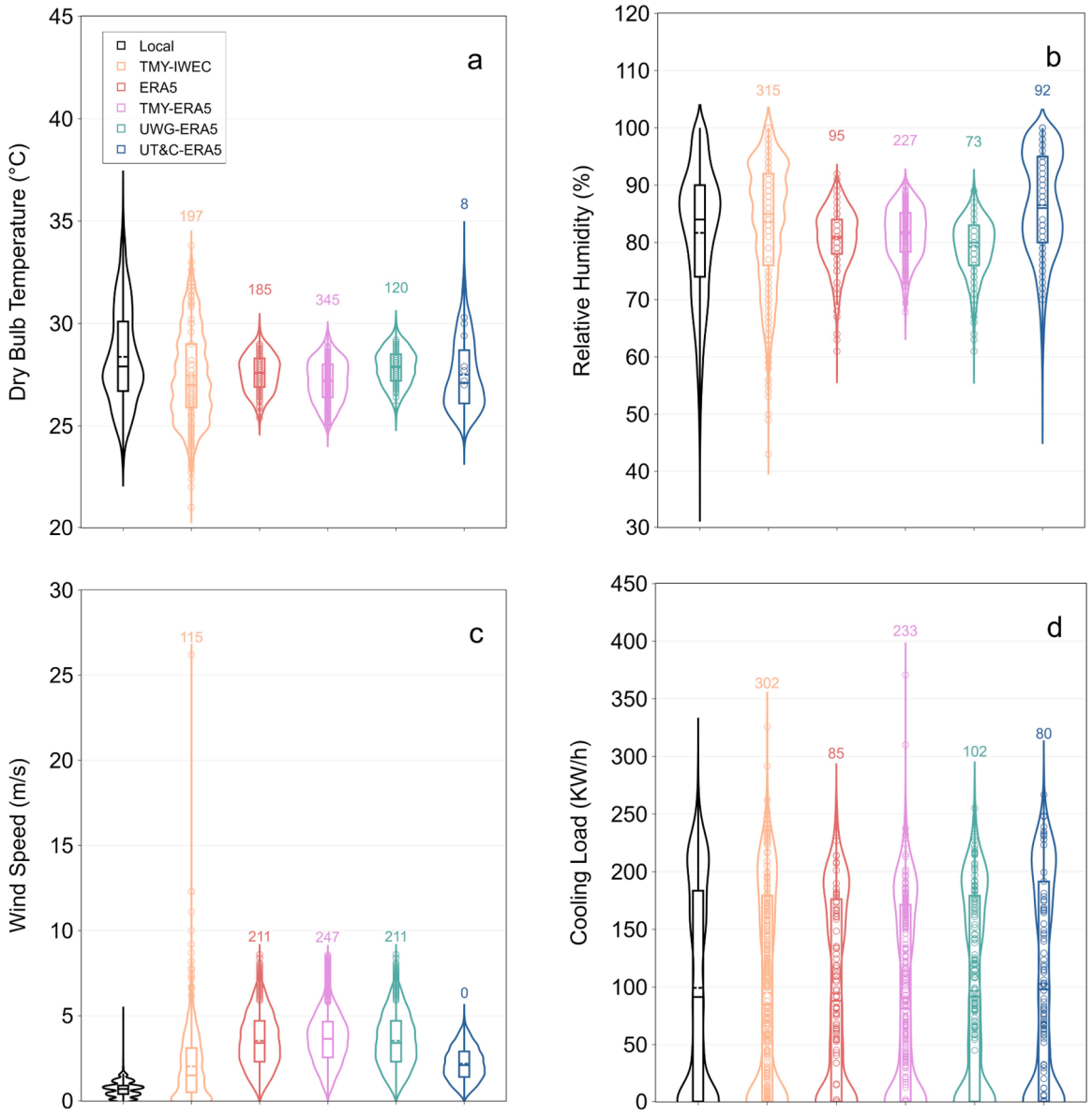

Fig. C. Hourly data distribution and outliers of (a) dry bulb temperature (b) relative humidity (c) wind speed (d) simulated cooling load for the entire study period. The outer contour of each violin represents the kernel density estimation (KDE) of the data distribution. The inner box embedded within the violin denotes the interquartile range (IQR). The dash horizontal line and solid horizontal line inside the box represent the mean value and the median value across all hours of the study period, respectively. The small circles are data points of outliers and the number above each violin represents the total number of outliers.

Fig. C shows the distribution of the hourly data and the number of outliers. The outliers are identified based on the 98th percentile of all the hourly data difference (40,080 data points in 8016 h from 5 datasets) compared to that in Local. Fig. C (a), (b) and (c) show the results of dry bulb temperature, relative humidity and wind speed. UT&C-ERA5 has least outliers in dry bulb temperature and wind speed, and UWG-ERA5 shows least outliers in relative humidity. For TMY datasets, results display more outliers in TMY-IWEC and TMY-ERA5 in temperature and humidity than other datasets. TMY-IWEC demonstrates fewer outliers in wind speed than the other datasets, except UT&C-ERA5, yet the outliers present are characterized by greater magnitude. Fig. C (d) shows the result of the simulated cooling load. TMY-IWEC demonstrates a close alignment in data distribution compared to Local but has the most outliers.

Data availability

Data will be made available on request.

References

"ERA5 hourly data on single levels from 1940 to present." https://cds.climate.copernicus.eu/datasets/reanalysis-era5-single-levels?tab=overview (accessed May. 26th, 2025).

Afshari, A. (2023). Optimization of urban design/retrofit scenarios using a computationally light standalone urban energy/climate model (SUECM) forced by ERA5 data. *Energy and Buildings, 287*. https://doi.org/10.1016/j.enbuild.2023.112991

Al-Hadhrami, L. M. (2013). Comprehensive review of cooling and heating degree days characteristics over Kingdom of Saudi Arabia. *Renewable and Sustainable Energy Reviews, 27*, 305–314. https://doi.org/10.1016/j.rser.2013.04.034

Aliabadi, A. A., Chen, X., Yang, J., Madadizadeh, A., & Siddiqui, K. (2023). Retrofit optimization of building systems for future climates using an urban physics model. *Building and Environment, 243*. https://doi.org/10.1016/j.buildenv.2023.110655

Allegrini, J., Dorer, V., & Carmeliet, J. (2012). Influence of the urban microclimate in street canyons on the energy demand for space cooling and heating of buildings. *Energy and Buildings, 55*, 823–832. https://doi.org/10.1016/j.enbuild.2012.10.013

Anselmo, S., Safaeianpour, A., Moghadam, S. T., & Ferrara, M. (2024). GIS-based solar radiation modelling for photovoltaic potential in cities: A sensitivity analysis for the evaluation of output variability range. *Energy Reports, 12*, 4656–4669. https://doi.org/10.1016/j.egyr.2024.10.031

ASHRAE, "ASHRAE Guideline 14-2014," 2014.

Aydin, E. E., Ortner, F. P., Peng, S., Yenardi, A., Chen, Z., & Tay, J. Z. (2024). Climate-responsive urban planning through generative models: Sensitivity analysis of urban planning and design parameters for urban heat island in Singapore's residential settlements. *Sustainable Cities and Society, 114*. https://doi.org/10.1016/j.scs.2024.105779

Barlow, J., et al. (2017). Developing a research strategy to better understand, observe, and simulate urban atmospheric processes at kilometer to subkilometer scales. *Bulletin of the American Meteorological Society, 98*(10). https://doi.org/10.1175/bams-D-17-0106.1. ES261-ES264.

Bourikas, L., et al. (2016). Transforming typical hourly simulation weather data files to represent urban locations by using a 3D urban unit representation with micro-climate simulations. *Future Cities and Environment, 2*(0). https://doi.org/10.1186/s40984-016-0020-4

Bre, F., e Silva Machado, R. M., Lawrie, L. K., Crawley, D. B., & Lamberts, R. (2021). Assessment of solar radiation data quality in typical meteorological years and its influence on the building performance simulation. *Energy and Buildings, 250*. https://doi.org/10.1016/j.enbuild.2021.111251

Brozovsky, J., Radivojevic, J., & Simonsen, A. (2022). Assessing the impact of urban microclimate on building energy demand by coupling CFD and building performance simulation. *Journal of Building Engineering, 55*. https://doi.org/10.1016/j.jobe.2022.104681

B. Bueno, "An urban weather generator coupling a building simulation program with an urban canopy model," 10/12 2010.

Bueno, B., Norford, L., Hidalgo, J., & Pigeon, G. (2012a). The urban weather generator. *Journal of Building Performance Simulation, 6*(4), 269–281. https://doi.org/10.1080/19401493.2012.718797

Bueno, B., Pigeon, G., Norford, L. K., Zibouche, K., & Marchadier, C. (2012b). Development and evaluation of a building energy model integrated in the TEB scheme. *Geoscientific Model Development, 5*(2), 433–448. https://doi.org/10.5194/gmd-5-433-2012

Cannon, D. J., Brayshaw, D. J., Methven, J., Coker, P. J., & Lenaghan, D. (2015). Using reanalysis data to quantify extreme wind power generation statistics: A 33 year case study in Great Britain. *Renewable Energy, 75*, 767–778. https://doi.org/10.1016/j.renene.2014.10.024

Causone, F., Corgnati, S. P., Filippi, M., & Olesen, B. W. (2010). Solar radiation and cooling load calculation for radiant systems: Definition and evaluation of the direct Solar load. *Energy and Buildings, 42*(3), 305–314. https://doi.org/10.1016/j.enbuild.2009.09.008

Chang, C., Chen, C.-Y., & Lin, T.-P. (2024). Combining geographic information and climate data to develop urban building energy prediction models in Taichung, Taiwan. *Sustainable Cities and Society, 117*. https://doi.org/10.1016/j.scs.2024.105949

Chong, A., Gu, Y., & Jia, H. (2021). Calibrating building energy simulation models: A review of the basics to guide future work. *Energy and Buildings, 253*. https://doi.org/10.1016/j.enbuild.2021.111533

Crawley, D. B., et al. (2001). EnergyPlus: Creating a new-generation building energy simulation program. *Energy and Buildings, 33*(4), 319–331. https://doi.org/10.1016/s0378-7788(00)00114-6

Cui, Y., Yan, D., Hong, T., Xiao, C., Luo, X., & Zhang, Q. (2017). Comparison of typical year and multiyear building simulations using a 55-year actual weather data set from China. *Applied Energy, 195*, 890–904. https://doi.org/10.1016/j.apenergy.2017.03.113

Dai, A. (2023). The diurnal cycle from observations and ERA5 in surface pressure, temperature, humidity, and winds. *Climate Dynamics, 61*(5–6), 2965–2990. https://doi.org/10.1007/s00382-023-06721-x

De Masi, R. F., Gigante, A., Ruggiero, S., & Vanoli, G. P. (2021). Impact of weather data and climate change projections in the refurbishment design of residential buildings in cooling dominated climate. *Applied Energy, 303*. https://doi.org/10.1016/j.apenergy.2021.117584

De Rosa, M., Bianco, V., Scarpa, F., & Tagliafico, L. A. (2014). Heating and cooling building energy demand evaluation; a simplified model and a modified degree days approach. *Applied Energy, 128*, 217–229. https://doi.org/10.1016/j.apenergy.2014.04.067

Desthieux, G., Gressin, A., Raybaud, B., & Ingensand, J. (2023). Solar potential on facades at urban scale: An integrated approach combining solar and digital building modelling. *Journal of Physics: Conference Series, 2600*(4). https://doi.org/10.1088/1742-6596/2600/4/042004

Detommaso, M., Costanzo, V., & Nocera, F. (2021). Application of weather data morphing for calibration of urban ENVI-met microclimate models. Results and critical issues. *Urban Climate, 38*. https://doi.org/10.1016/j.uclim.2021.100895

Dougherty, T. R., & Jain, R. K. (2023). Invisible walls: Exploration of microclimate effects on building energy consumption in New York City. *Sustainable Cities and Society, 90*. https://doi.org/10.1016/j.scs.2022.104364

Duarte, C., Raftery, P., & Schiavon, S. (2017). Development of whole-building energy models for detailed energy insights of a large office building with green certification rating in Singapore. *Energy Technology, 6*(1), 84–93. https://doi.org/10.1002/ente.201700564

Energy Market Authority. "Chapter 3: Energy consumption." https://www.ema.gov.sg/resources/singapore-energy-statistics/chapter3 (accessed Mar. 11, 2024).

B. Erdman. "Modern-era retrospective analysis for Research and Applications, version 2." https://gmao.gsfc.nasa.gov/reanalysis/MERRA-2/(accessed May. 26th, 2025).

Fatichi, S., Ivanov, V. Y., & Caporali, E. (2011). Simulation of future climate scenarios with a weather generator. *Advances in Water Resources, 34*(4), 448–467. https://doi.org/10.1016/j.advwatres.2010.12.013

Gobakis, K., & Kolokotsa, D. (2017). Coupling building energy simulation software with microclimatic simulation for the evaluation of the impact of urban outdoor conditions on the energy consumption and indoor environmental quality. *Energy and Buildings, 157*, 101–115. https://doi.org/10.1016/j.enbuild.2017.02.020

Grimmond, C. S. B., et al. (2009). Urban surface energy balance models: Model characteristics and methodology for a comparison study. In A. Baklanov, G. Sue, M. Alexander, & M. Athanassiadou (Eds.), *Meteorological and air quality models for urban areas* (pp. 97–123). Berlin, Heidelberg: Springer Berlin Heidelberg.

Gualtieri, G. (2021). Reliability of ERA5 reanalysis data for wind resource assessment: A comparison against tall towers. *Energies, 14*(14). https://doi.org/10.3390/en14144169

Hadavi, M., & Pasdarshahri, H. (2021a). Investigating effects of urban configuration and density on urban climate and building systems energy consumption. *Journal of Building Engineering, 44*. https://doi.org/10.1016/j.jobe.2021.102710

Hadavi, M., & Pasdarshahri, H. (2021b). Impacts of urban buildings on microclimate and cooling systems efficiency: Coupled CFD and BES simulations. *Sustainable Cities and Society, 67*. https://doi.org/10.1016/j.scs.2021.102740

Hashemi, F., Mills, G., Poerschke, U., Iulo, L. D., Pavlak, G., & Kalisperis, L. (2024). A novel parametric workflow for simulating urban heat island effects on residential building energy use: Coupling local climate zones with the urban weather generator a case study of seven U.S. cities. *Sustainable Cities and Society, 110*. https://doi.org/10.1016/j.scs.2024.105568

Hersbach, H., et al. (2020). The ERA5 global reanalysis. *Quarterly Journal of the Royal Meteorological Society, 146*. https://doi.org/10.1002/qj.3803, 06/15.

H. Hersbach and National Center for Atmospheric Research Staff (Eds). "The Climate Data Guide: ERA5 atmospheric reanalysis." https://climatedataguide.ucar.edu/climate-data/era5-atmospheric-reanalysis (accessed Sept 3, 2024).

Hu, M., Ghorbany, S., Yao, S., & Wang, C. (2024). Micro-urban heatmapping: A multi-modal and multi-temporal data collection framework. *Buildings, 14*(9). https://doi.org/10.3390/buildings14092751

Huang, Y. J., Su, F., Seo, D., & Krarti, M. (2014). Development of 3012 IWEC2 weather files for international locations (RP-1477). *ASHRAE Transactions, 120*, 340–355, 01/01.

Ibrahim, A. J., Zangana, D. D., Liu, S., Samuelson, H., & Yang, L. (2025). Impacts of climate change on energy-saving sensitivity of residential building envelope design parameters in three hot-dry cities. *Journal of Building Engineering, 99*. https://doi.org/10.1016/j.jobe.2024.111481

Ignatius, M., Wong, N. H., & Jusuf, S. K. (2016). The significance of using local predicted temperature for cooling load simulation in the tropics. *Energy and Buildings, 118*, 57–69. https://doi.org/10.1016/j.enbuild.2016.02.043

International Renewable Energy Agency, "Breakthrough agenda report 2023," Paris, 2023.

Järvi, L., Grimmond, C. S. B., & Christen, A. (2011). The surface urban energy and water balance Scheme (SUEWS): Evaluation in Los Angeles and Vancouver. *Journal of Hydrology, 411*(3–4), 219–237. https://doi.org/10.1016/j.jhydrol.2011.10.001

Jiang, Q., et al. (2021a). Evaluation of the ERA5 reanalysis precipitation dataset over Chinese Mainland. *Journal of Hydrology, 595*. https://doi.org/10.1016/j.jhydrol.2020.125660

Jiang, R., Li, W., Lu, X. X., Xie, J., Zhao, Y., & Li, F. (2021b). Assessment of temperature extremes and climate change impacts in Singapore, 1982–2018. *Singapore Journal of Tropical Geography, 42*(3), 378–396. https://doi.org/10.1111/sjtg.12384

Jiao, D., Xu, N., Yang, F., & Xu, K. (Sep 9 2021). Evaluation of spatial-temporal variation performance of ERA5 precipitation data in China. *Scientific Reports, 11*(1), Article 17956. https://doi.org/10.1038/s41598-021-97432-y

Jin, L., Schubert, S., Fenner, D., Meier, F., & Schneider, C. (2020). Integration of a building energy model in an urban climate model and its application. *Boundary-Layer Meteorology, 178*(2), 249–281. https://doi.org/10.1007/s10546-020-00569-y

Kamal, A., et al. (2021). Impact of urban morphology on urban microclimate and building energy loads. *Energy and Buildings, 253*. https://doi.org/10.1016/j.enbuild.2021.111499

Kokkonen, T. V., et al. (2018). Sensitivity of surface urban energy and water balance scheme (SUEWS) to downscaling of reanalysis forcing data. *Urban Climate, 23*(2), 36–52. https://doi.org/10.1016/j.uclim.2017.05.001

Kondo, H., Genchi, Y., Kikegawa, Y., Ohashi, Y., Yoshikado, H., & Komiyama, H. (2005). Development of a multi-layer urban canopy model for the analysis of energy consumption in a big City: Structure of the urban canopy model and its basic performance. *Boundary-Layer Meteorology, 116*(3), 395–421. https://doi.org/10.1007/s10546-005-0905-5

Lee, D.-I., & Lee, S.-H. (2020). The microscale urban surface energy (MUSE) model for real urban application. *Atmosphere, 11*(12). https://doi.org/10.3390/atmos11121347

Li, Q., Wang, W., Yu, Z., & Chen, J. (2023). Assessing urban micro-climates with vertical and horizontal building morphological cutting deep transfer learning neural networks. *Building and Environment, 234*. https://doi.org/10.1016/j.buildenv.2023.110186

Li, Q., Xu, G., & Gu, Z. (2024). A novel framework for multi-city building energy simulation: Coupling urban microclimate and energy dynamics at high spatiotemporal resolutions. *Sustainable Cities and Society, 113*. https://doi.org/10.1016/j.scs.2024.105718

Lipson, M. J., et al. (2023a). Evaluation of 30 urban land surface models in the Urban-PLUMBER project: Phase 1 results. *Quarterly Journal of the Royal Meteorological Society*. https://doi.org/10.1002/qj.4589

Lipson, M. J., et al. (2023b). Evaluation of 30 urban land surface models in the Urban-PLUMBER project: Phase 1 results. *Quarterly Journal of the Royal Meteorological Society, 150*(758), 126–169. https://doi.org/10.1002/qj.4589

Liu, S., Kwok, Y. T., & Ren, C. (2023b). Investigating the impact of urban microclimate on building thermal performance: A case study of dense urban areas in Hong Kong. *Sustainable Cities and Society, 94*. https://doi.org/10.1016/j.scs.2023.104509

Liu, S., Wang, Y., Liu, X., Yang, L., Zhang, Y., & He, J. (2023a). How does future climatic uncertainty affect multi-objective building energy retrofit decisions? Evidence from residential buildings in subtropical Hong Kong. *Sustainable Cities and Society, 92*. https://doi.org/10.1016/j.scs.2023.104482

Liu, X., et al. (2024). A novel quantitative method of heatwave classification for building resilience analysis. *Sustainable Cities and Society, 112*. https://doi.org/10.1016/j.scs.2024.105603

Liu, Y., Stouffs, R., Tablada, A., Wong, N. H., & Zhang, J. (2017). Comparing micro-scale weather data to building energy consumption in Singapore. *Energy and Buildings, 152*, 776–791. https://doi.org/10.1016/j.enbuild.2016.11.019

Masson, V., Grimmond, S., & Oke, T. (2002). Evaluation of the town energy balance (TEB) scheme with direct measurements from dry districts in two cities. *Journal of Applied Meteorology*. https://doi.org/10.1175/1520-0450(2002)041<1011:EOTTEB>2.0.CO;2, 10/01.

Mei, S.-J., & Yuan, C. (2021). Analytical and numerical study on transient urban street air warming induced by anthropogenic heat emission. *Energy and Buildings, 231*. https://doi.org/10.1016/j.enbuild.2020.110613

Meili, N., et al. (2020). An urban ecohydrological model to quantify the effect of vegetation on urban climate and hydrology (UT&C v1.0). *Geoscientific Model Development, 13*(1). https://doi.org/10.5194/gmd-13-335-2020

Miguel, M., et al. (2021). A physically-based model of interactions between a building and its outdoor conditions at the urban microscale. *Energy and Buildings, 237*. https://doi.org/10.1016/j.enbuild.2021.110788

Miller, C., Thomas, D., Kämpf, J., & Schlueter, A. (2017). Urban and building multiscale co-simulation: Case study implementations on two university campuses. *Journal of Building Performance Simulation, 11*(3), 309–321. https://doi.org/10.1080/19401493.2017.1354070

Miniandi, N. D., Muhammad, M. K. I., Jamal, M. H., & Shahid, S. (2024). Urbanization signature on hourly rainfall extremes of Kuala Lumpur. *Sustainable Cities and Society, 112*. https://doi.org/10.1016/j.scs.2024.105610

M'Saouri El Bat, A., Romani, Z., Bozonnet, E., & Draoui, A. (2021). Thermal impact of street canyon microclimate on building energy needs using TRNSYS: A case study of the city of Tangier in Morocco. *Case Studies in Thermal Engineering, 24*. https://doi.org/10.1016/j.csite.2020.100834

Oke, T. R., Mills, G., Christen, A., & Voogt, J. A. (2017). *Urban climates*. Cambridge University Press.

Palme, M., Inostroza, L., Villacreses, G., Lobato, A., & Carrasco, C. (2017). Urban weather data and building models for the inclusion of the urban heat island effect in building performance simulation. *Data in Brief, 14*, 671–675. https://doi.org/10.1016/j.dib.2017.08.035. Oct.

R. Paolini and M. Santamouris, *Urban Climate change and heat islands*. 2023.

Qian, B., Yu, T., Zhang, C., Heiselberg, P., Lei, B., & Yang, L. (2023). A method of determining typical meteorological year for evaluating overheating performance of passive buildings. *Building Simulation, 16*(4), 511–526. https://doi.org/10.1007/s12273-022-0967-z, 2023/04/01.

Richards, P. J., & Hoxey, R. P. (1993). Appropriate boundary conditions for computational wind engineering models using the k-ϵ turbulence model. *Journal of Wind Engineering and Industrial Aerodynamics, 46-47*, 145–153. https://doi.org/10.1016/0167-6105(93)90124-7

Rutten, D. (2013). Galapagos: On the logic and limitations of generic solvers. *Architectural Design, 83*(2), 132–135. https://doi.org/10.1002/ad.1568

Shan, X., Luo, N., Sun, K., Hong, T., Lee, Y.-K., & Lu, W.-Z. (2020). Coupling CFD and building energy modelling to optimize the operation of a large open office space for occupant comfort. *Sustainable Cities and Society, 60*. https://doi.org/10.1016/j.scs.2020.102257

Shen, P., et al. (2025a). Climate adaptability of building passive strategies to changing future urban climate: A review. *Nexus, 2*(2). https://doi.org/10.1016/j.ynexs.2025.100061

Shen, P. (2025a). Building and urban simulation under future climate: A novel statistical downscaling method for future hourly weather data generation. *Building Simulation*. https://doi.org/10.1007/s12273-025-1277-z

Shen, P., et al. (2025b). Recent progress in building energy retrofit analysis under changing future climate: A review. *Applied Energy, 383*. https://doi.org/10.1016/j.apenergy.2025.125441

Shen, P., Liu, J., & Wang, M. (2021). Fast generation of microclimate weather data for building simulation under heat island using map capturing and clustering technique. *Sustainable Cities and Society, 71*. https://doi.org/10.1016/j.scs.2021.102954

Shen, P., Wang, M., Liu, J., & Ji, Y. (2023). Hourly air temperature projection in future urban area by coupling climate change and urban heat island effect. *Energy and Buildings, 279*. https://doi.org/10.1016/j.enbuild.2022.112676

Shen, P., & Yang, B. (2020). Projecting Texas energy use for residential sector under future climate and urbanization scenarios: A bottom-up method based on twenty-year regional energy use data. *Energy, 193*. https://doi.org/10.1016/j.energy.2019.116694

Silvero, F., Lops, C., Montelpare, S., & Rodrigues, F. (2019). Generation and assessment of local climatic data from numerical meteorological codes for calibration of building energy models. *Energy and Buildings, 188-189*, 25–45. https://doi.org/10.1016/j.enbuild.2019.02.001

Singapore Productivity and Standards Board. "Code of practice for mechanical ventilation and air-conditioning in buildings." Spring Singapore, Singapore, p. 2001. https://www.singaporestandardseshop.sg/Product/SSPdtDetail/8690d588-7d33-42e5-a541-d0f684f966fe (accessed 13th Nov 2024).

Spiridonov, V., & Ćurić, M. (2021). Atmospheric pressure and wind. In V. Spiridonov, & M.Ćurić Eds (Eds.), *Fundamentals of meteorology* (pp. 87–114). Cham: Springer International Publishing.

Sun, Y., & Augenbroe, G. (2014). Urban heat island effect on energy application studies of office buildings. *Energy and Buildings, 77*, 171–179. https://doi.org/10.1016/j.enbuild.2014.03.055

Tang, Y., et al. (2021). Urban meteorological forcing data for building energy simulations. *Building and Environment, 204*. https://doi.org/10.1016/j.buildenv.2021.108088

Tian, X., Zhang, H., Liu, L., Huang, J., Liu, L., & Liu, J. (2024). Establishment of LCZ-based urban building energy consumption dataset in hot and humid subtropical regions through a bottom-up method. *Applied Energy, 368*. https://doi.org/10.1016/j.apenergy.2024.123491

Toparlar, Y., Blocken, B., Maiheu, B., & van Heijst, G. J. F. (2018). Impact of urban microclimate on summertime building cooling demand: A parametric analysis for Antwerp, Belgium. *Applied Energy, 228*, 852–872. https://doi.org/10.1016/j.apenergy.2018.06.110

Tsonis, A. A., Pan, X., Wang, G., & Nicolis, C. (2019). On the min–max estimation of mean daily temperatures. *Climate Dynamics, 53*(3–4), 1981–1989. https://doi.org/10.1007/s00382-019-04757-6

Wang, C., et al. (2022). Efficient cooling of cities at global scale using urban green space to mitigate urban heat island effects in different climatic regions. *Urban Forestry & Urban Greening, 74*. https://doi.org/10.1016/j.ufug.2022.127635

Wong, N. H., et al. (2021). An integrated multiscale urban microclimate model for the urban thermal environment. *Urban Climate, 35*. https://doi.org/10.1016/j.uclim.2020.100730

Wu, Y., An, J., Gui, C., Xiao, C., & Yan, D. (2023). A global typical meteorological year (TMY) database on ERA5 dataset. *Building Simulation, 16*(6), 1013–1026. https://doi.org/10.1007/s12273-023-1015-3

Xu, L., et al. (2022). Better understanding on impact of microclimate information on building energy modelling performance for urban resilience. *Sustainable Cities and Society, 80*. https://doi.org/10.1016/j.scs.2022.103775

Yang, X., Zhao, L., Bruse, M., & Meng, Q. (2012). An integrated simulation method for building energy performance assessment in urban environments. *Energy and Buildings, 54*, 243–251. https://doi.org/10.1016/j.enbuild.2012.07.042

Yang, Y., Gu, Q., Wei, H., Liu, H., Wang, W., & Wei, S. (2023). Transforming and validating urban microclimate data with multi-sourced microclimate datasets for building energy modelling at urban scale. *Energy and Buildings, 295*. https://doi.org/10.1016/j.enbuild.2023.113318

Yuan, C., Adelia, A. S., Mei, S., He, W., Li, X.-X., & Norford, L. (2020). Mitigating intensity of urban heat island by better understanding on urban morphology and anthropogenic heat dispersion. *Building and Environment, 176*. https://doi.org/10.1016/j.buildenv.2020.106876

Yuan, Y., Li, C., Geng, X., Yu, Z., Fan, Z., & Wang, X. (2022). Natural-anthropogenic environment interactively causes the surface urban heat island intensity variations in global climate zones. *Environment International, 170*, Article 107574. https://doi.org/10.1016/j.envint.2022.107574. Dec.

Zhang, M., & Gao, Z. (2021). Effect of urban form on microclimate and energy loads: Case study of generic residential district prototypes in Nanjing, China. *Sustainable Cities and Society, 70*. https://doi.org/10.1016/j.scs.2021.102930

Zhang, R., & Mirzaei, P. A. (2020). CFD-CFD coupling: A novel method to develop a fast urban microclimate model. *Journal of Building Physics, 44*(5), 385–408. https://doi.org/10.1177/1744259120935921

Zhang, Y., Teoh, B. K., & Zhang, L. (2024). Multi-objective optimization for energy-efficient building design considering urban heat island effects. *Applied Energy, 376*. https://doi.org/10.1016/j.apenergy.2024.124117

Zheng, X., Chen, L., & Yang, J. (2023). Simulation framework for early design guidance of urban streets to improve outdoor thermal comfort and building energy efficiency in summer. *Building and Environment, 228*. https://doi.org/10.1016/j.buildenv.2022.109815

Zou, J., et al. (2022). Performance of air temperature from ERA5-land reanalysis in coastal urban agglomeration of Southeast China. *Science Total Environment, 828*, Article 154459. https://doi.org/10.1016/j.scitotenv.2022.154459. Jul 1.